Inorganic Chemistry

Article

pubs.acs.org/IC

Hydrido Copper Clusters Supported by Dithiocarbamates: Oxidative Hydride Removal and Neutron Diffraction Analysis of $[Cu_7(H)\{S_2C(aza\text{-}15\text{-}crown\text{-}5)\}_6]$

Ping-Kuei Liao,[†] Ching-Shiang Fang,[†] Alison J. Edwards,[‡] Samia Kahlal,[§,⊥] Jean-Yves Saillard,*[,§,⊥] and C. W. Liu*[,†]

[†]Department of Chemistry, National Dong Hwa University, Hualien, Taiwan 97401, R. O. C.

[‡]Bragg Institute, Australian Nuclear Science and Technology Organisation, Lucas Heights, NSW Australia

[§]UMR-CNRS 6226 "Institut des Sciences Chimiques de Rennes", Université de Rennes 1, 35042 Rennes cedex, France

[⊥]Université Européenne de Bretagne, 5 bd. Laënnec, 35000 Rennes, France

Supporting Information

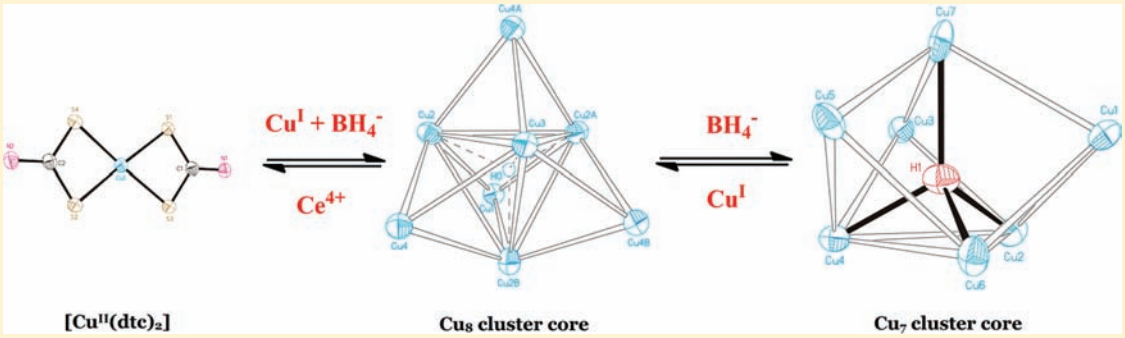

ABSTRACT: Reactions of Cu(I) salts with $Na(S_2CR)$ (R = N^nPr_2, NEt_2, aza-15-crown-5), and $(Bu_4N)(BH_4)$ in an 8:6:1 ratio in CH_3CN solution at room temperature yield the monocationic hydride-centered octanuclear Cu^I clusters, $[Cu_8(H)\{S_2CR\}_6](PF_6)$ (R = N^nPr_2, $\mathbf{1_H}$; NEt_2, $\mathbf{2_H}$; aza-15-crown-5, $\mathbf{3_H}$). Further reactions of $[Cu_8(H)\{S_2CR\}_6](PF_6)$ with 1 equiv of $(Bu_4N)(BH_4)$ produced neutral heptanuclear copper clusters, $[Cu_7(H)\{S_2CR\}_6]$ (R = N^nPr_2, $\mathbf{4_H}$; NEt_2, $\mathbf{5_H}$; aza-15-crown-5, $\mathbf{6_H}$) and clusters **4**–**6** can also be generated from the reaction of $Cu(BF_4)_2$, $Na(S_2CR)$, and $(Bu_4N)(BH_4)$ in a 7:6:8 molar ratio in CH_3CN. Reformation of cationic Cu^I_8 clusters by adding 1 equiv of Cu^I salt to the neutral Cu_7 clusters in solution is observed. Intriguingly, the central hydride in $[Cu_8(H)\{S_2CN^nPr_2\}_6](PF_6)$ can be oxidatively removed as H_2 by $Ce(NO_3)_6^{2-}$ to yield $[Cu^{II}(S_2CN^nPr_2)_2]$ exploiting the redox-tolerant nature of dithiocarbamates. Regeneration of hydride-centered octanuclear copper clusters from the $[Cu^{II}(S_2CN^nPr_2)_2]$ can be achieved by reaction with Cu(I) ions and borohydride. The hydride release and regeneration of Cu^I_8 was monitored by UV–visible titration experiments. To our knowledge, this is the first time that hydride encapsulated within a copper cluster can be released as H_2 via chemical means. All complexes have been fully characterized by ^{1}H NMR, FT-IR, UV–vis, and elemental analysis, and molecular structures of $\mathbf{1_H}$, $\mathbf{2_H}$, and $\mathbf{6_H}$ were clearly established by single-crystal X-ray diffraction. Both $\mathbf{1_H}$ and $\mathbf{2_H}$ exhibit a tetracapped tetrahedral Cu_8 skeleton, which is inscribed within a S_{12} icosahedron constituted by six dialkyl dithiocarbamate ligands in a tetrametallic-tetraconnective (μ_2, μ_2) bonding mode. The copper framework of $\mathbf{6_H}$ is a tricapped distorted tetrahedron in which the four-coordinate hydride is demonstrated to occupy the central site by single crystal neutron diffraction. Compounds **1**–**3** exhibit a yellow emission in both the solid state and in solution under UV irradiation at 77 K, and the structureless emission is assigned as a ^{3}metal to ligand charge transfer (MLCT) excited state. Density functional theory (DFT) and time-dependent density functional theory (TDDFT) calculations on model compounds match the experimental structures and provide rationalization of their bonding and optical properties.

INTRODUCTION

The chemistry of metal hydrides has been heavily pursued because these molecules are key intermediates in various catalytic reactions.[1] Metal hydrides have promising applications as new materials for hydrogen storage.[2] In this regard, conversion of dihydrogen into a metal hydride and liberation of the hydride as dihydrogen via chemical means represents an attractive and safe method of hydrogen storage.[3] Understanding the chemistry of metal hydride species is thus central to the design of new materials for hydrogen storage.

The metallic hydrides are frequently referred to as interstitial hydrides due to the fact that hydrogen occupies interstitial sites in the metal host lattice. Four-coordinate hydrogen in

Received: January 18, 2012
Published: June 4, 2012

   dx.doi.org/10.1021/ic300135w | Inorg. Chem. 2012, 51, 6577–6591

Scheme 1. Preparation of Complexes 1−7

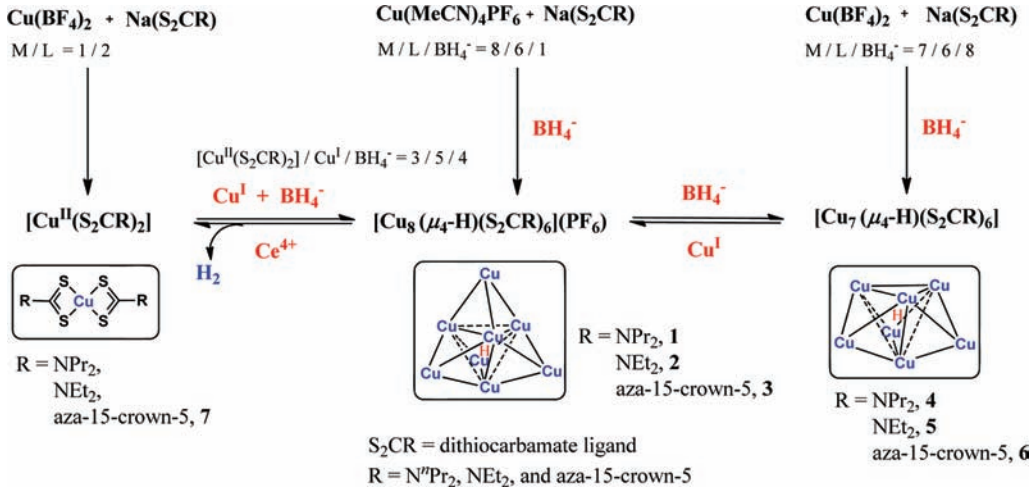

tetrahedral sites and six-coordinate hydrogen in octahedral sites are those most commonly observed in intermetallic hydrides.[2b] In molecular compounds, six-coordinate hydrogen in an octahedral cavity has been well studied for example $[Cu_6(H)(Cl)\{Me_3(NCH_2)_3\}_3]^+$,[4] $[Cr_6(\mu_3\text{-}S)_8(H)(PEt_3)_6]$,[5] $[Ru_7(CO)_{19}(\mu\text{-}CNMe_2)(\mu_6{-}H)]$,[6] $[HRu_6(CO)_{18}]^-$,[7] $[HCo_6(CO)_{15}]^-$,[8] and $[HNi_{12}(CO)_{21}]^{3-}$.[9] The latter three structures were elucidated by single-crystal neutron analysis. Surprisingly it was not until 2008 that the first molecular species containing a 4-coordinate hydrogen in the tetrahedral cavity of $[(C_5Me_4SiMe_3)YH_2]_4(THF)$ was characterized via neutron diffraction.[10] Other examples of 4-coordinate hydrogen in a tetrahedral hole are $[(C_5Me_4SiMe_3)LuH_2]_4$,[11] $[(Tp^{Me2})LnH_2]_4$ (Ln = Y, Nd, Sm, Lu),[12] $[\{Rh_2(PNNP)(CO)_2\}_2(\mu_4\text{-}H)]$ (PNNP = 3,5-bis(diphenylphosphinomethyl)pyrazolate],[13] $[(C_5Me_4SiMe_3Lu)_4(\mu\text{-}NH_2)_7(\mu_4\text{-}H)]$,[14] $[\{PhP(CH_2)_3Fe\}_4(\mu_4\text{-}H)]^-$,[15] and $[(^tBuCH_2O)_{12}Mo_4(\mu_4\text{-}H)]^-$.[16]

Despite numerous reports of transition metal clusters with an interstitial hydride located at either tetrahedral or octahedral sites, surprisingly, very few compounds from which interstitial hydride can be released as dihydrogen by chemical methods have been established. The lability of interstitial hydrides is controversial. It has been reported that the oxidation of $[Cr_6(\mu_3\text{-}S)_8(H)(PEt_3)_6]$[5] with ferrocenium tetrafluoroborate affords $[Cr_6(\mu_3\text{-}S)_8(H)(PEt_3)_6](BF_4)$ while the hydride remains in the center of Cr_6 octahedron.[17] On the other hand, the interstitial hydrides in some octahedral complexes have been noted to be mobile between the center of the octahedron and the cluster surface. For instance, the central hydride in $[Ru_6(\mu_6\text{-}H)(CO)_{18}]^-$ is stable in both a methanol solution of KOH and a THF solution of KH, but protonation of $[Ru_6(\mu_6\text{-}H)(CO)_{18}]^-$ affords $H_2Ru_6(CO)_{18}$, with two bridging hydrides.[18] The interstitial hydride in $[HCo_6(CO)_{15}]^-$ undergoes an intriguing rapid migration from the inside to the outside of the cluster.[19] The 4-coordinate hydrogen atom in a tetrahedral cavity identified in $[(C_5Me_4SiMe_3)LnH_2]_4(THF)$ (Ln = Y, Gd, Dy, Lu) seems to be quite stable despite the observation that these rare-earth polyhydrido complexes show excellent olefin-polymerization activity.[20] The reaction of tetranuclear rare-earth metal octahydrido complexes $[(C_5Me_4SiMe_3)LuH_2]_4(THF)$ with ammonia yields selectively the heptaamido-monohydrido complexes $[\{(C_5Me_4SiMe_3)Lu\}_4(\mu\text{-}NH_2)_6(\mu_3\text{-}NH_2)(\mu_4\text{-}H)]$, in which a μ_4-H ligand remains at the center of the tetrahedral metal framework.[14] Exposure of this heptaamido-monohydrido complex to an ammonia atmosphere at room temperature for two days affords the octaamido complex $[(C_5Me_4SiMe_3)Lu(\mu\text{-}NH_2)]_4$ quantitatively.[14] Apparently H_2 was released on ammonolysis.

Recently reported hydride-centered octanuclear copper/silver clusters, $[M_8(H)\{E_2P(OR)_2\}_6]^+$ (M = Cu, Ag; E = S, Se)[21] and $[M_8(H)\{S_2CC(CN)_2\}_6]^{5-}$ (M = Cu, Ag),[22] are a new class of 4-coordinate H atom lying in the center of a tetracapped tetrahedral (or triakis-tetrahedral)[23] metallic cavity inscribed within a distorted E_{12} icosahedron. The encapsulated hydride is extraordinarily stable, and this stability can be attributed to strong bonding interactions between the central hydride and encapsulating Cu(I)/Ag(I) ions. The strong interaction and small radius of hydride induces a tetrahedral contraction of the cubic metallic framework. In the search for hydride activation within copper clusters, the redox-tolerant dithiocarbamate ligands were pursued with the hope that the central hydride can be abstracted oxidatively to release dihydrogen. Herein the syntheses, redox, and photophysical properties of a series of hydrido copper clusters stabilized by dialkyl dithiocarbamates as well as their hydride abstraction and addition reactions are described. Also reported is the single crystal neutron diffraction analysis of $[Cu_7(H)\{S_2C(aza\text{-}15\text{-}crown\text{-}5)\}_6]$ from which the central hydride is unequivocally proven to occupy a central tetrahedral site.

RESULTS AND DISCUSSION

The synthetic details of hydrido-copper clusters stabilized by dithiocarbamate (dtc) ligands as well as their redox reactions en route to the formation of either heptanuclear copper clusters or mononuclear Cu(II) species from octanuclear Cu(I) complexes are described in Scheme 1. The hydride (or deuteride) encapsulated compounds (**1**, **2**, and **3**) can be produced by the reaction of $[Cu(CH_3CN)_4](PF_6)$, $Na(S_2CR)$ (R = N^nPr_2, **1**; NEt_2, **2**; aza-15-crown-5, **3**), and $(^nBuN_4)(BH_4)$ or $(^nBuN_4)(BD_4)$ in an 8:6:1 molar ratio in CH_3CN solution. Unlike other hydrido-copper clusters stabilized by six dichalcogenophosphate ligands which can also be synthesized from the hydride insertion into the empty copper homocubane, the formation of compounds **1**−**3** via this method is not an easy task. In 2006, Hogarth et al. reported the structure of dicationic $[Cu_8\{S_2CN^nPr_2\}_6]^{2+}$,[24] which contains an empty Cu^I_8 cubic cage capped by six dipropyl dithiocarbamate ligands

dx.doi.org/10.1021/ic300135w | Inorg. Chem. 2012, 51, 6577−6591

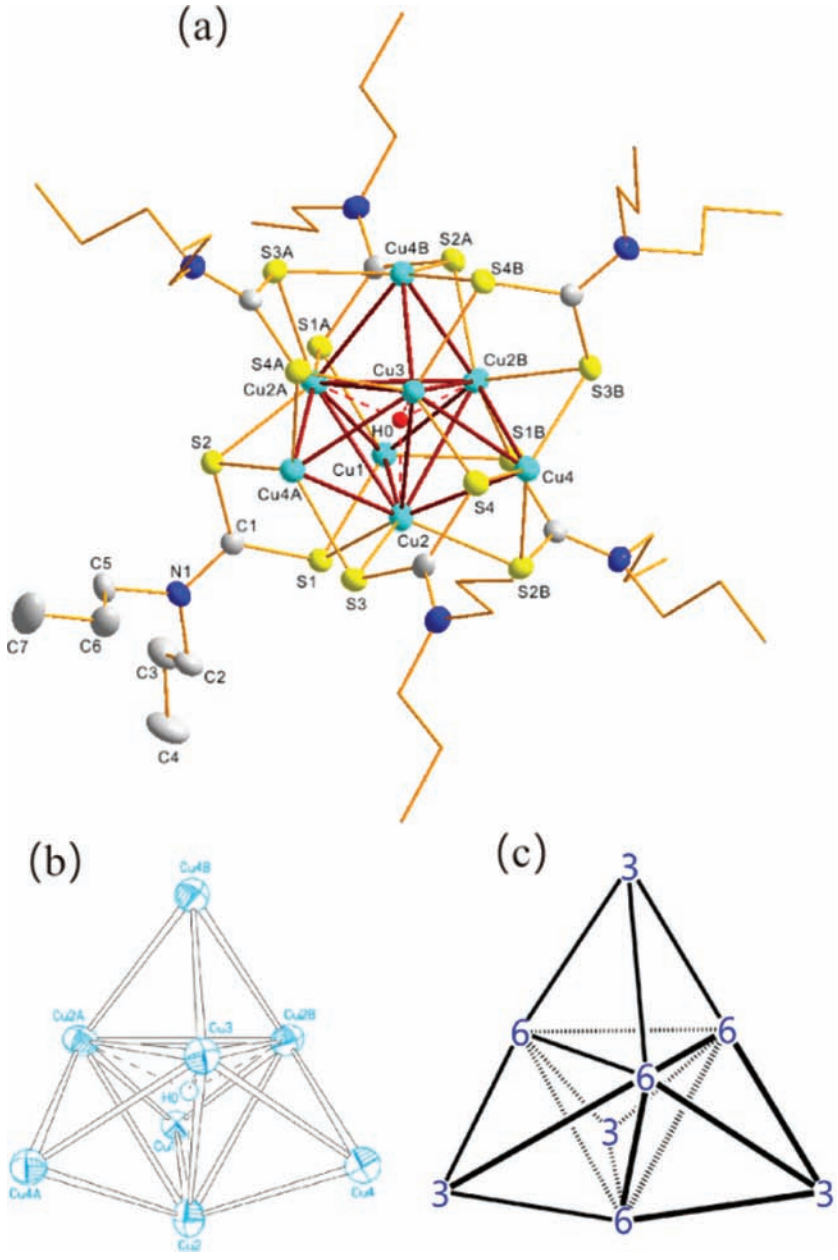

Figure 1. (a) Molecular structure of the cationic $[Cu_4(\mu_4\text{-H})(\mu_3\text{-Cu})_4\{S_2CN^nPr_2\}_6]^+$ in $\mathbf{1_H}$. H-atoms omitted for clarity except the central hydride. (b) Central unit of $[Cu_8H]$ in $\mathbf{1_H}$. (c) Tetracapped tetrahedron with numbers in the vertices indicating their degrees.

$(S_2CN^nPr_2)^-$, in a μ_4 bridging pattern on each square face of a cube. In contrast, the octanuclear copper clusters $[Cu_8\{S_2P(OR)_2\}_6]^{2+}$ [21a] and $[Cu_8\{Se_2P(OR)_2\}_6]^{2+}$,[21b] can be readily prepared by the direct reaction of copper salts and dichalcogenophosphate ligands in a 4:3 ratio, whereas $[Cu_8\{S_2CN^nPr_2\}_6]^{2+}$ could not be generated by this methodology. The difficulty in the isolation of pure cluster $[Cu_8\{S_2CN^nPr_2\}_6]^{2+}$ discouraged synthesis of **1**−**3** via the hydride insertion reaction. Nevertheless the empty cubane, $[Cu_8\{S_2CN^nPr_2\}_6]^{2+}$, can be reasonably proposed as a labile intermediate, en route to the final products **1**−**3** on the basis of the known reaction pathways in the formation of dichalcogenophosphato copper clusters with an encapsulated hydride.

Since the dithiocarbamate-type ligands are both innocent and redox-tolerant, they have the potential to stabilize high oxidation state metal complexes[25] so we were curious about the further reaction products of clusters **1**−**3** with borohydrides. To our great surprise, the hydride-centered (or deuteride-centered) Cu^I_7 clusters surrounded by six dithiocarbamate ligands, **4**, **5**, and **6** can be isolated from the reaction of **1**−**3** with $(Bu_4N)(BH_4)$ within 1 h, respectively (Scheme 1). Compounds **4**, **5**, and **6** can also be isolated by the reaction of $Cu(BF_4)_2$, $Na(S_2CR)$, and $(^nBuN_4)(BH_4)$ in a 7:6:8 molar ratio in CH_3CN in 10 min. Here each Cu^{II} is reduced to Cu^I by 1 equiv of BH_4^- anion and a further equivalent of BH_4^- anion provides the hydride to generate Cu^I_7 clusters. More importantly, the Cu^I_7 clusters can be easily converted to Cu^I_8 clusters by adding 1 equiv of a Cu^I salt to the Cu^I_7 compounds in solution.

We have demonstrated that the hydride-centered copper clusters stabilized by dichalcogenophosphate ligands are exceedingly stable even on addition of stoichiometric amounts of strong acid or base such as HBF_4 or NaOH with prolonged stirring.[21a,b] No decomposition was detected as the line shape

dx.doi.org/10.1021/ic300135w | Inorg. Chem. 2012, 51, 6577−6591

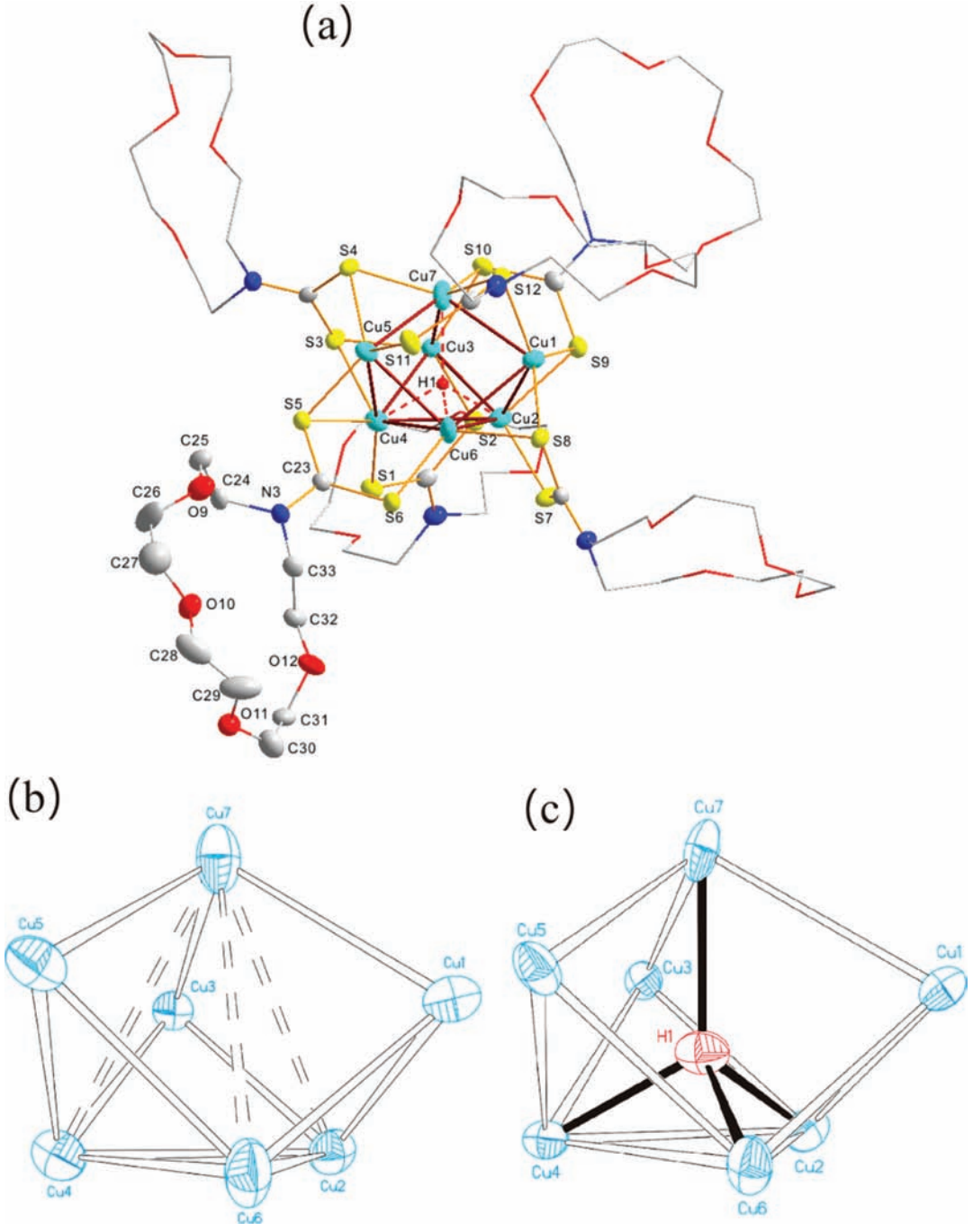

Figure 2. (a) Molecular structure of the $[Cu_4(\mu_4\text{-}H)(\mu_3\text{-}Cu)_3\{S_2C(\text{aza-15-crown-5})\}_6]$ in $\mathbf{6_H}$. H-atoms omitted for clarity except the interstitial hydride. (b) Cu_7 skeleton of $\mathbf{6_H}$ displays a tricapped pyramid. (c) Cu_7H core drawing from neutron diffraction data.

of broad hydride resonance in ^{1}H NMR spectra remains unchanged. Gratifyingly, the hydride of Cu_8H clusters ($\mathbf{1_H}$, $\mathbf{2_H}$, and $\mathbf{3_H}$) can be oxidatively removed only after adding the oxidizing agent, $(NH_4)_2[Ce(NO_3)_6]$, with conversion of the cluster to $[Cu^{II}(S_2CR)_2]$, **7**, and vice versa. The titration reactions which demonstrate the hydride uptake and release can be monitored by UV−vis spectroscopy. More importantly, the hydrido Cu^I_8 clusters can be regenerated from CH_3CN solutions containing $[Cu^{II}(S_2CR)_2]$ and Cu^I sources (in the form of $[Cu(CH_3CN)_4](PF_6)$ in a 3:5 molar ratio with 4 equiv of BH_4^- anion; Scheme 1).

All the spectroscopic characteristics and main structural features of the new compounds **1**−**7** as well as their redox and photophysical properties are described below:

Crystallography: Compound $\mathbf{1_H}$. The monocationic octanuclear copper cluster crystallizes in the trigonal space group, $P\bar{3}1c$, with a solvating $CHCl_3$ and a PF_6^- anion per cluster. Unlike previously reported hydrido copper complexes,[21] none of the copper atoms of this cluster are disordered, but the PF_6^- anion is disordered over two equivalent positions. The central Cu_8 core is arranged in a tetracapped-tetrahedral (or triakis-tetrahedral) geometry[23] about a 3-fold axis on which the hydrogen must lie and is stabilized by twelve μ_2-S atoms from six dithiocarbamate (dtc) ligands in a distorted

dx.doi.org/10.1021/ic300135w | Inorg. Chem. 2012, 51, 6577−6591

icosahedral geometry (Figure 1a). One Cu(3) atom and three Cu(2) (abbreviated as Cu_v) atoms form an inner tetrahedron and are directly connected to the inferred central hydride. Each face of the inner tetrahedron is capped either by the Cu(1) or by one of the three Cu(4) atoms (abbreviated as Cu_{cap}) of an outer tetrahedron (Figure 1b). The Cu_v–Cu_{cap} [2.577(1)–2.669(1) Å] distances are much shorter than the sum of the van der Waals radii for copper atoms (2.80 Å)[26] and are shorter than the Cu_v–Cu_v distances 2.894(2)–2.989(2) Å. The average Cu–Cu distance [2.806(1) Å] in the Cu_8 empty cluster, $[Cu_8\{S_2CN^nPr_2\}_6]^{2+}$,[24] lies between Cu_v–Cu_{cap} and Cu_v–Cu_v of complex $\mathbf{1_H}$. The average Cu_v-inferred central μ-H distance [1.80(12) Å] is slightly shorter than that observed in $[Cu_8(H)\{S_2P(O^iPr)_2\}_6]^+$ [1.831(3) Å][20] and longer than the sum of their covalent radii [1.63(5) Å].[27] Six dtc ligands, each adopting a tetrametallic, tetraconnective (μ_2-S, μ_2-S) bonding mode, are located on the top of Cu_4 butterflies where the hinge positions are the edge of the inner tetrahedron and the wingtips are the four capping Cu atoms (Figure 1a). The inner Cu atoms in $\mathbf{1_H}$ are proposed to possess a tetrahedral S_3H coordination, while the capping Cu atoms have trigonal planar S_3 coordination. The dihedral angles of Cu_4 butterflies range from 153.2° to 157.8°. Two kinds of Cu–S distances, namely, Cu_v–S and Cu_{cap}–S, each averaging 2.358(2) and 2.270(2) Å, are revealed in $\mathbf{1_H}$ with the shorter being to the wingtip Cu atoms (Cu_{cap}).[21,22] The Cu_{cap}–S distances lie in the same range as those observed in the octanuclear cubic copper cluster $[Cu_8\{S_2CN^nPr_2\}_6]^{2+}$ [2.246(2)Å],[24] and the average intraligand S···S bite distance, 3.066(2) Å, is likewise comparable to 3.082(1) Å.[24] The C–S distances in the range of 1.741(5)–1.747(5) Å are marginally shorter than those observed in $[Cu_8\{S_2CN^nPr_2\}_6]^{2+}$ [1.752(3)–1.754(3) Å].[24]

Heteroelemental cages having a tetracapped-tetrahedron or distorted-cubic framework are not unusual. The $[Fe_4S_4]$ moiety,[28] ubiquitously present in the core unit of ferredoxin, is one of the most studied metal chalcogenide skeletons in bioinorganic chemistry. Nevertheless homometallic clusters containing this geometry have only been reported in metallocarbohedranes such as Ti_8C_{12},[29] observed in the gas phase only, and no guest atom was observed in the center. The tetracapped tetrahedral core does exist in the heterometallic cluster, $[Os_4(CO)_{12}\{Pd(P^tBu_3)\}_4]$,[30a] and $[E_4(PdL_2)_4]^{2+}$ (L = PPh_2Me; E = Sb or Bi)[30b] involving a tetrahedral core E_4 (E = Sb or Bi) with four PdL_2 as capping groups. Examples also include $[Cu_4Mn_4(S^nPr)_{12}S]^{2-}$ [31] and $[Re_4(CO)_{12}\{\mu_3\text{-InRe}(CO)_5\}_4]$.[32] A schematic drawing of a tetracapped tetrahedron with the degree of vertex represented by number is displayed in Figure 1c.

Compound $\mathbf{2_H}$. The ethyl homologue, $\mathbf{2_H}$, crystallizes in the cubic $Pn\bar{3}n$ space group. The geometry of the copper skeleton is a tetracapped tetrahedron of T_d symmetry corresponding to a cube in which alternate corners are displaced along the 3-fold toward the center, and the eight Cu^I ions are further surrounded by six dtc ligands (Supporting Information Figure S1). The whole copper skeleton is disordered over two positions. The vertices of the tetrahedron are formed by the Cu1, Cu4C, Cu4D, and Cu4E atoms, and the capping atoms are Cu3A, Cu3, Cu3B, and Cu2A (or vice versa). The edge lengths of the tetrahedron (Cu_v–Cu_v), 2.854(4) and 3.003(4)Å, are larger than Cu_v–Cu_{cap} [2.492(4)—2.659(3) Å]; however, those distances are slightly less than those (Cu_v–Cu_v and Cu_v–Cu_{cap}) observed in $\mathbf{1_H}$. Similar to $\mathbf{1_H}$, the dtc ligands adopt a tetrametallic–tetraconnective (μ_2, μ_2) bonding mode to cap a Cu_4 butterfly formed by two Cu_{cap} and two Cu_v atoms. The average dihedral angle of Cu_4 butterflies [156.23(11)°] is analogous to those in $\mathbf{1_H}$. The presence of a central hydride is inferred from spectroscopic measurements and is proposed to lie at the center of the cube 1.795(2) Å from the surrounding Cu atoms for $\mathbf{2_H}$.

Compound $\mathbf{6_H}$. The neutral heptanuclear copper cluster crystallizes in the triclinic $P\bar{1}$ space group, with one cluster and one acetone molecule per asymmetric unit. The cluster contains a distorted, tricapped tetrahedral copper core centered about an interstitial hydride anion and is surrounded by six aza-15-crown-5-dtc ligands (Figure 2a). Compared with the tetracapped tetrahedral copper skeleton of $\mathbf{1_H}$, this tricapped-tetrahedral copper skeleton $\mathbf{6_H}$ (Figure 2b) appears to arise from losing one capping copper atom of $\mathbf{1_H}$. The central tetrahedron, which approaches a triangular pyramid arising from a pseudo-C_3 elongation, is formed by Cu2, Cu4, Cu6, and Cu7 atoms (abbreviated as Cu_v), and the three capping atoms are Cu1, Cu3, and Cu5 (abbreviated as Cu_{cap}). The basal plane of atoms Cu2, Cu4, and Cu6 lacks a capping Cu atom. The elongated edges of the pyramid range from 3.373(2)–3.403(1) Å, the average length of the basal plane edge is 2.726(1) Å, which is slightly shorter than the sum of the van der Waals radii for two copper atoms, 2.8 Å, and is longer than Cu_v–Cu_{cap} [av. 2.616(2)] of compound $\mathbf{1_H}$. Of the six aza-15-crown-5-dtc ligands, only two achieve a tetrametallic–tetraconnective (μ_2-S; μ_2-S) bonding mode and are located on the top of Cu_4 butterflies where hinge positions are elongated edges of the triangular pyramid and wingtips are capping Cu atoms. The other four dtc ligands exist in a trimetallic, triconnective (μ_2-S; μ_1-S) bonding mode. One is capping the remaining Cu_4 butterfly above the basal plane with a nonbonding Cu6—S11, 3.067(2) Å, and the other three are located about the uncapped Cu_3 basal plane linking two vertices and one capping Cu atom. Thus the Cu6 presents a trigonal planar S_2H coordination. Twelve sulfur atoms form a distorted icosahedral cage with an average, intraligand S···S bite distance of 3.041(2) Å. *This constitutes the first Cu_7 cluster within an S_{12} icosahedron.*

The central hydride atom position of $\mathbf{6_H}$ is unequivocally proven by single-crystal neutron diffraction (Figure 2c), and it is well-defined when refined anisotropically. This unambiguous determination of H atom positions reveals bond lengths of Cu_v–H as Cu2–H1 = 1.81(2) Å, Cu4–H1 = 1.84(2) Å, Cu6–H1 = 1.78(2) Å, Cu7–H1 = 2.02(2) Å, and a Cu_{cap}–H distance (Cu3–H1) of 2.21(2) Å. This clear differentiation of the Cu_v atoms from the Cu_{cap} atoms is in stark contrast to the negligible resolution of these particular features by X-ray diffraction. Clearly, only the four Cu_v (Cu2, Cu4, Cu6, Cu7) atoms display bonding interactions with the central hydride. The distortion away from ideal tetrahedral geometry is observed in the bond angles at H(1) which range from 94.3(13) to 120.2(15)°. The mean Cu–(μ_4-H) distance [1.86(2) Å] of $\mathbf{6_H}$ is somewhat longer than the 1.76(3) Å (average), observed in a three-coordinate hydride in $[Cu_6(P(p\text{-tolyl})_3)(\mu_3\text{-H})]_6$ determined by neutron diffraction analysis.[33]

Considering the geometry of the Cu_7 skeleton only, this tricapped tetrahedral core does occur in several homometallic and heterometallic clusters. Examples are $[Cu_7Te\{As(Te_2)(Te_2)\}_3]^{4-}$,[34] $[Co_7S_6(PPh_3)_5Cl_2]$,[35] $[Au_3Ru_4(\mu\text{-H})(CO)_{12}(PPh_3)_3]$,[36] $[Au_3CoRu_3(CO)_{12}(PPh_3)_3]$,[37] $[Bi_4Fe_4(CO)_{13}]^-$,[38] and $[Os_5(CO)_{12}Ru(\eta^5\text{-}C_5H_5)(AuPPh_3)]$.[39]

NMR Studies of Compounds 1–6. The ^1H NMR spectra display a set of chemical shifts corresponding to the propyl,

dx.doi.org/10.1021/ic300135w | Inorg. Chem. 2012, 51, 6577–6591

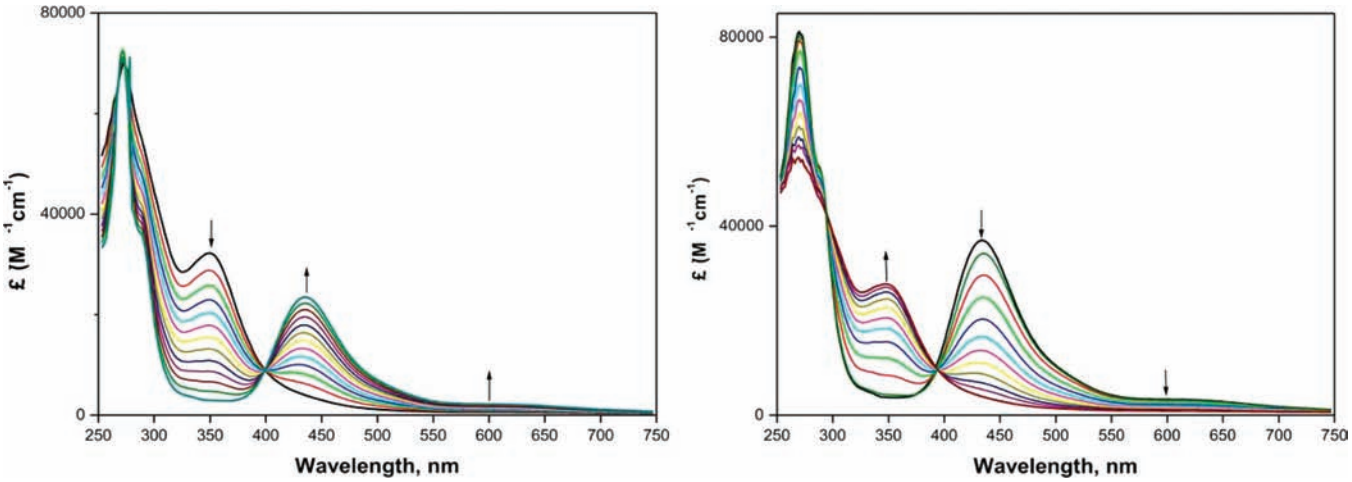

Figure 3. (left) Absorption spectral changes of $\mathbf{1_H}$ (6.6×10^{-5} M) upon addition of the $(NH_4)_2[Ce(NO_3)_6]$ [$(0-5.28) \times 10^{-4}$ M] in 50% (v/v) $CH_3CN-CH_2Cl_2$. (right) Back titrations of $(Bu_4N)(BH_4)$ [$(0.44-5.28) \times 10^{-4}$ M] in 50% (v/v) $CH_3CN-CH_2Cl_2$.

ethyl, and aza-15-crown-5 groups respectively for each of the compounds in the series. Compound $\mathbf{1_H}$ shows a broad peak centered at 7.05 ppm that integrates to $\mathbf{1_H}$ relative to 12 methylene protons of the propyl groups. Peak broadening is attributed to coupling to adjacent quadrupolar copper nuclei (I = 3/2). In a similar manner $\mathbf{2_H}$ and $\mathbf{3_H}$ also gave a resonance for encapsulated hydride at 7.02 and 7.03 ppm, respectively. The presence of deuteride in the analogous deuterium species ($\mathbf{1_D}-\mathbf{3_D}$) was confirmed via ^{2}H NMR. $\mathbf{1_D}$ exhibits a peak at 7.07 ppm corresponding to the entrapped deuteride, while $\mathbf{2_D}$ and $\mathbf{3_D}$ gave the same deuteride chemical shifts at 7.02 ppm. These observed values are markedly different from hydride chemical shifts of $[Cu_8(H)\{Se_2P(OR)_2\}_6]^+$ [21b] and $[Cu_8(H)\{S_2P(OR)_2\}_6]^+$,[21a] at −0.58 and 3.69 ppm, respectively, but comparable to $[Cu_8(H)\{S_2CC(CN)_2\}_6]^{5-}$,[22] at 7.60 ppm. The PF_6^- counteranion in compounds **1**−**3** is clearly observed by ^{31}P NMR spectroscopy. The hydride in the Cu_7 ($\mathbf{4_H}-\mathbf{6_H}$) clusters and their deuterium analogues ($\mathbf{4_D}-\mathbf{6_D}$) is observed. Compounds $\mathbf{4_H}$ and $\mathbf{5_H}$ both gave encapsulated hydride resonances at 6.55 and 6.49 ppm. $\mathbf{4_D}$, $\mathbf{5_D}$, and $\mathbf{6_D}$ show deuteride peaks at 6.40, 6.50, and 6.51 ppm, respectively. No PF_6^- counteranion was detected in the ^{31}P NMR spectrum of compounds **4**−**6**, and these compounds are thus demonstrated to be neutral species. A slightly downfield shift of ∼0.5 ppm for the hydride resonance of octanuclear copper(I) clusters ($\mathbf{1_H}$, $\mathbf{2_H}$, and $\mathbf{3_H}$) is revealed by comparison with the hydride resonance of heptanuclear copper(I) clusters ($\mathbf{4_H}$, $\mathbf{5_H}$, and $\mathbf{6_H}$). Since the absorption spectra of hydride-encapsulated Cu^I_8 or Cu^I_7 clusters are almost the same (vide infra), NMR spectrometry is the best spectroscopic tool to differentiate these two clusters. The hydride downfield shift of the octanuclear species relative to the heptanuclear one is reproduced by our DFT calculations for models of $[Cu_4(\mu_4\text{-}H)Cu_4\{S_2CNH_2\}_6]^+$ and $[Cu_4(\mu_4\text{-}H)Cu_3(S_2CNH_2)_6]$ (vide infra).

Copper Uptake by the Clusters $[Cu_7(H)\{S_2CR_2\}_6]$. The cationic Cu^I_8 clusters, **1**−**3**, can be converted to the neutral Cu^I_7 clusters, **4**−**6**, upon the reaction of $(Bu_4N)(BH_4)$/$(Bu_4N)(BD_4)$ with the octanuclear copper-hydrido complexes. The reactions were monitored by ^{1}H NMR spectroscopy and representative spectra are given in Supporting Information Figure S2. After the addition of 1 equiv of $(Bu_4N)(BH_4)$ to the NMR tube containing $[Cu_8(H)\{S_2CN^nPr_2\}_6](PF_6)$, $\mathbf{1_H}$, with a hydride resonance at 7.05 ppm, ^{1}H NMR spectra were recorded at 5 min intervals and a new peak was observed at 6.55 ppm, corresponding to the hydride resonance of the neutral cluster $[Cu_7(H)\{S_2CN^nPr_2\}_6]$, $\mathbf{4_H}$. The integration ratio of these two peaks centered at 7.05 and 6.55 ppm relative to the methylene protons of the six propyl groups is also approximately 1−12 at each time step. Thus, in this process, no other hydrido copper species were detected. The Cu^I_8 can be completely converted to Cu^I_7 cluster over 50 min. The hydride resonance corresponding to $[Cu_8(H)\{S_2CN^nPr_2\}_6]^+$ species was detected in the ^{1}H NMR spectrum immediately upon addition of 1 equiv $[Cu(CH_3CN)_4](PF_6)$ to the NMR tube containing $[Cu_7(H)\{S_2CN^nPr_2\}_6]$. It is thus demonstrated that a copper ion can be released from the cluster cation, $[Cu_8(H)(S_2CR_2)_6]^+$, or taken up by the neutral Cu_7 species, mediated by the reducing agent or Cu^I salt (Scheme 1), respectively. The redox-tolerant nature of the dtc ligands where the whole copper skeleton encapsulated can stabilize both Cu_8H and Cu_7H frameworks and facilitates interconversion.

Mass Spectrometry. Molecular ion peaks of **1**−**3** were readily identified from the positive ESI-mass spectrometry [1568.1 (1569.2) for $\mathbf{1_H}$ ($\mathbf{1_D}$), 1400.8 (1402.5) for $\mathbf{2_H}$ ($\mathbf{2_D}$), and 2275.4 (2276.7) for $\mathbf{3_H}$ ($\mathbf{3_D}$)]. The experimental isotopic distribution pattern of both hydride and deuteride compounds are in good agreement with the theoretical ones and representative patterns of $\mathbf{1_H}$ and $\mathbf{1_D}$ are given in Supporting Information Figure S3. The molecular ion peak, $[Cu_7(H)(dtc)_6 + H^+]$, of $Cu_7H(dtc)_6$ clusters, 1504.8 for $\mathbf{4_H}$, 1336.5 for $\mathbf{5_H}$, and 2213.3 for $\mathbf{6_H}$, are not observed by positive ESI-mass spectrometry. Instead, peaks for which m/z correspond to the whole molecular species with an additional copper ion to form the adduct ion, $[\{Cu_7(H)(dtc)_6\}(Cu)]^+$, are identified. This is quite unexpected and implies that the neutral Cu_7H clusters are not being stable in the ESI gas phase conditions. Indeed the reaction of the heptanuclear copper cluster with a copper ion forms the cationic, hydrido Cu^I_8 cluster as reported above.

Hydride Abstraction and Addition Monitored by UV−vis. The UV−vis titration experiments of a series of $[Cu_8(H)\{S_2CR\}_6]^+$ complexes with $(NH_4)_2[Ce(NO_3)_6]$ and the further backtitration with $(Bu_4N)(BH_4)$ have been studied. All the complexes exhibit similar phenomena and representative spectra of compound $\mathbf{1_H}$ are given in Figure 3. The UV−vis spectrum of $\mathbf{1_H}$ in 50% (v/v) $CH_3CN-CH_2Cl_2$ solution

dx.doi.org/10.1021/ic300135w | Inorg. Chem. 2012, 51, 6577−6591

showed intense bands centered at 276 and 345 nm. Figure 3 illustrates the absorption spectral changes of $\mathbf{1_H}$ upon the addition of $(NH_4)_2[Ce(NO_3)_6]$ (forward reaction, left) and the addition of $(Bu_4N)(BH_4)$ (backward reaction, right). The absorbance of the visible band at 345 nm gradually decreases upon stepwise addition of $(NH_4)_2[Ce(NO_3)_6]$ while a new band maximum at 430 nm and a low-energy tail at 600 nm with low extinction coefficient, progressively increase. The new absorption bands at ~430 nm can be tentatively assigned to a ligand to metal charge transfer (LMCT) band[40] and at ~600 nm, a symmetry forbidden LMCT transition (vide infra). The reaction sequence can be represented as eqs 1−3 shown below:

$$[Cu_8(H)(S_2CR)_6]^+ + Ce^{4+} \rightarrow [Cu_8(S_2CR)_6]^{2+} + 0.5H_2 + Ce^{3+} \quad (1)$$

$$[Cu_8(S_2CR)_6]^{2+} + 3Ce^{4+} \rightarrow 3[Cu^{II}(S_2CR)_2] + 5Cu^+ + 3Ce^{3+} \quad (2)$$

$$3[Cu^{II}(S_2CR)_2] + 5Cu^+ + 4BH_4^- \rightarrow [Cu_8(H)(S_2CR)_6]^+ + 2(B_2H_6) + 1.5H_2 \quad (3)$$

The reaction of $(NH_4)_2[Ce(NO_3)_6]$ with $\mathbf{1_H}$ was monitored by ^{1}H NMR which reveals that within 5 min the central hydride peak at 7.05 ppm disappears and after 30 min the ligand related peaks are also broadened. Reaction of the oxidant was evident with liberation of hydrogen gas from the hydrido copper(I) clusters on the formation of empty cubane cluster $[Cu_8\{S_2CN^nPr_2\}_6]^{2+}$ (eq 1 determined by GC-MS; Supporting Information Figure S4). We propose $[Cu_8\{S_2CN^nPr_2\}_6]^{2+}$ has been formed upon oxidation of $\mathbf{1_H}$. In the presence of oxidant, it has proven extremely difficult to stop the reaction at this step or fully characterize this sequence. The empty Cu_8 cube can be further oxidized to become $[Cu^{II}(S_2CN^nPr_2)_2]$ (eq 2). We have nevertheless managed to theoretically reproduce the UV−vis absorption spectrum of $[Cu_8\{S_2CNR_2\}_6]^{2+}$ by DFT modeling (vide infra). The calculated absorption spectrum shows little difference from that of compound **1**. The reversed process in which UV−vis spectra are measured to follow the stepwise titration of $(Bu_4N)(BH_4)$. This suggests that the dual functions of BH_4^- anion as both a reducing agent to reduce Cu^{II} to Cu^I and a hydride donor to form the hydrido Cu^I_8 cluster.

The entrapped hydride is quite stable in $[Cr_6S_8(H)(PEt_3)_6]$ which can be further oxidized by $(FeCp_2)(BF_4)$ to produce one-electron oxidized cluster $[Cr_6S_8(H)(PEt_3)_6]^+$.[17] However, the oxidizer (Ce^{IV}) we used was much stronger than $[FeCp_2]^+$,[41] and clearly, this forces the oxidization to proceed to yield H_2 and $[Cu^{II}(S_2CR)_2]$ species.

In order to prove that the inverse UV−vis titration experiments apply in bulk, we undertook an experiment combining $[Cu^{II}(S_2CN^nPr_2)_2]$ and $[Cu(CH_3CN)_4](PF_6)$ in the ratio of 3:5 in CH_3CN followed by the addition of 4 equiv of $(Bu_4N)(BH_4)$ (eq 3). The initial deep brown solution turned yellow over ca. 3 min with the concomitant formation of gas bubbles in the solution, which suggests that H_2 gas was formed. After 10 min stirring, the species in solution was confirmed as the hydride-encapsulated Cu^I_8 cluster by ^{1}H NMR. On further addition of 1 equiv of $(Bu_4N)(BH_4)$ (total 5 equiv), the color of the mixture turned orange over 5 min, and the solution was subsequently characterized to contain the hydride-encapsulated Cu^I_7 cluster by ^{1}H NMR spectroscopy. Thus 1 equiv more of BH_4^- reduces one of the copper atoms in $\mathbf{1_H}$ to form $\mathbf{4_H}$. The reaction of $Cu(BF_4)_2$ and $Na(S_2CN^nPr_2)$ in a 7:6 ratio in CH_3CN followed by the addition of 8 equiv of $(Bu_4N)(BH_4)$ produces pure $\mathbf{4_H}$ in high yield (eq 4). These studies thus reveal a new synthetic route for the preparation of pure hydride-centered Cu^I_8 and Cu^I_7 clusters.

$$7Cu^{2+} + 6(S_2CR)^- + 8BH_4^- \rightarrow [Cu_7(H)(S_2CR)_6] + 4(B_2H_6) + 3.5H_2 \quad (4)$$

Cyclic Voltammograms of 1−6. Cyclic voltammograms of the hydride-centered Cu^I_8 and Cu^I_7 clusters surrounded by six dithiocarbamate ligands display similar irreversible Cu^I/Cu^{II} oxidation and they are summarized in Table 2. The electrochemical oxidation of $\mathbf{1_H}$ has been investigated at room temperature in 50% (v/v) $CH_3CN-CH_2Cl_2$ solution [0.1 M $(Bu_4N)(ClO_4)$] at 100 mV s^{-1} for the oxidation of 5 mM of compound $\mathbf{1_H}$ using a glassy carbon working electrode. $\mathbf{1_H}$ exhibits an irreversible wave at 0.36 V which indicates the formation of the Cu^{II} species (Figure 4). The small peak at 0.06 V suggests the reduction of Cu^{II} species to Cu^I species.

When the scan rate was decreased, the Cu^{II}/Cu^I reduction was decreased. The peak position shifts upon variation of the scan rate. This suggests that oxidation occurs alongside a rapid chemical process. Appearance of a brown coloration is observed near the working electrode, which suggests decomposition of the compound during the redox process. After running several cycles of the redox process, the UV−vis spectra of the experimental solution show a new visible band at 430 nm consistent with the formation of $[Cu^{II}(dtc)_2]$ species. Owing to the decomposition of the Cu^I_8 hydride cluster and the gradual loss of hydride during the oxidation, the hydrido clusters cannot be regenerated in the cyclic voltammetry experiments.

Photophysical Properties of 1−3. The photophysical data including UV−vis, excitation, and emission of compounds $\mathbf{1_H}-\mathbf{3_H}$ are summarized in Table 3. The spectral profiles of all compounds are quite similar and representative spectra of $\mathbf{1_H}$ are displayed in Figure 5. The electronic absorption spectrum of $\mathbf{1_H}$ in CH_2Cl_2 displays an intense absorption band at 276 (ε = 68 000 cm^{-1} M^{-1}) nm and a less intense band at about 345 (ε = 37 000 cm^{-1} M^{-1}) nm (Figure 5a). The origin of the high-energy band is likely to be a ligand-centered transition, as the sodium salts of dithiocarbamate exhibit absorptions in this region (260 and 291 nm).[42] The low-energy band could be tentatively assigned to the metal to ligand charge transfer (MLCT) transition (vide infra). The compound $\mathbf{1_H}$ exhibits a yellow emission in both the solid state and solution under UV−irradiation at 77 K. Direct excitation of the low energy band resulted in a broad, structureless emission centered at 576 nm (Figure 5b). In frozen and degassed CH_2Cl_2, the emission band is centered at 591 nm (Figure 5c), which is red-shifted about ~15 nm compared to the emission from the solid state. A large Stoke shift (>12 600 cm^{-1}) and the long emission lifetimes of **1−3** implied the possibility of a large distortion in the excited state and emission from a spin-forbidden triplet emissive state. The broad, featureless nature of the emission band of $\mathbf{1_H}$ is consistent with a ^{3}MLCT excited state. This is consistent with our TDDFT calculations (vide infra). To the best of our knowledge no reports on the emissive properties of any copper dithiocarbamate complexes have ever been communicated. Of course the photochemistry of Cu(II) dithiocarbamate in CCl_4 has been well established.[43]

Theoretical Investigations: $[Cu_8(H)\{S_2CNH_2\}_6]^+$. The major computed data associated with the optimized structure

dx.doi.org/10.1021/ic300135w | Inorg. Chem. 2012, 51, 6577−6591

Table 1. Selected Bond Lengths (Å) and Angle (deg) with Estimated Standard Deviations Listed in Parentheses

	$\mathbf{1}_H$	$\mathbf{2}_H$	$\mathbf{6}_H$	$\mathbf{6}_H$ (neutron)
Cu_v-H^a	1.74(3), 1.99(12)	1.780(2), 1.838(2)	1.78(6), 1.83(6), 1.86(6), 2.09(6)	1.84(2), 1.81(2), 1.78(2), 2.02(2)
$Cu_v-Cu_v{}^b$	2.894(2), 2.895(2), 2.989(2)	3.003(4), 2.854(4)	2.660(1), 2.907(1), 2.612(1), 3.373(2), 3.403(1), 3.378(1)	2.864(13), 2.633(14), 2.605(13), 3.349(17), 3.335(15), 3.290(17)
$Cu_v-Cu_{cap}{}^c$	2.593(1), 2.669(1), 2.576(1), 2.653(1), 2.577(1)	2.492(4), 2.559(2), 2.634(3), 2.659(3)	2.570(1), 2.609(1), 2.751(1), 2.550(1), 2.572(1), 2.588(1), 2.681(1), 2.651(1), 2.571(1)	2.608(14), 2.601(13), 2.750(13), 2.575(13), 2.577(12), 2.544(14), 2.677(14), 2.621(15), 2.548(13)
Cu_v-S	2.324(2), 2.368(2), 2.388(2), 2.352(2)	2.394(2), 2.360(2), 3.378(2), 3.450(2)	2.261(2), 2.339(2), 2.459(2), 2.267(2), 2.350(2), 2.655(2), 2.278(2), 2.286(2), 2.333(2), 2.240(2), 2.373(2), 3.067(2)	2.36(2), 2.23(3), 2.48(3),2.26(3), 2.63(3), 2.37(3),2.30(2), 2.29(3), 2.35(3),2.26(3), 2.38(2), 3.01(4)
$Cu_{cap}-S$	2.277(2), 2.256(2), 2.271(2), 2.278(2)	2.190(2), 2.212(2), 2.241(2), 2.250(2)	2.258(2), 2.267(2), 2.285(2), 2.255(2), 2.270(2), 2.285(2), 2.222(2), 2.276(2), 2.336(2)	2.25(2), 2.27(3), 2.28(3),2.34(2), 2.28(3), 2.22(3)2.38(2), 2.27(3), 2.24(3)
S···S (bite)	3.064(2), 3.067(2)	3.064(2)	3.031(2), 3.030(2), 3.035(2), 3.048(2), 3.050(2), 3.051(2)	2.97(4), 3.02(4), 3.10(3),3.10(4), 3.06(3), 3.05(4)
C–S [average]	1.741(5)–1.747(5) [1.744(5)]	1.735(5)–1.747(5) [1.741(5)]	1.703(5)–1.756(5) [1.732(5)]	1.68(3)–1.76(3) [1.72(3)]
dihedral angles of the Cu_4 butterfly	153.19(4), 157.84(4)	153.21(10), 159.24(11)	149.33(4), 161.49(4), 164.23(4)	148.7(5), 160.7(6), 161.4(6)

[a] H atom positions inferred from symmetry and spectroscopic considerations except for $\mathbf{6}_H$ (neutron) which are determined. [b] Cu_v = Cu atoms at the vertex of the tetrahedron. [c] Cu_{cap} = Cu atoms capped to the tetrahedron face

Table 2. Redox Potential (V vs $FeCp_2{}^{0/+}$) of Compounds $\mathbf{1}_H-\mathbf{6}_H{}^a$

compd	E_{pA}	E_{pB}	compd	E_{pA}	E_{pB}
$\mathbf{1}_H$	0.36	0.06	$\mathbf{4}_H$	0.35	0.08
$\mathbf{2}_H$	0.34	0.07	$\mathbf{5}_H$	0.38	0.10
$\mathbf{3}_H$	0.38	0.04	$\mathbf{6}_H$	0.33	0.05

[a] At a glassy-carbon electrode, scan rate 100 mV s^{-1}

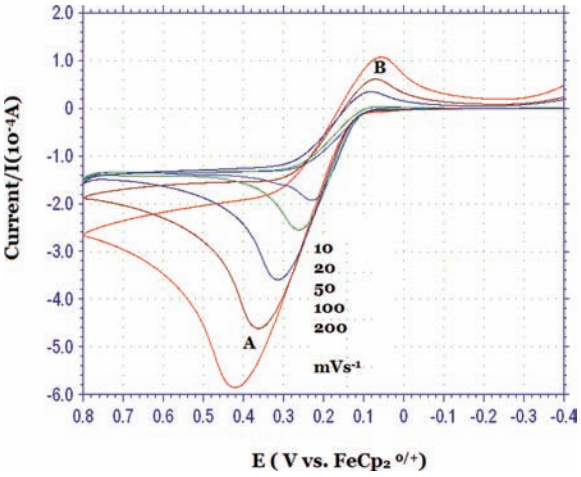

Figure 4. Cyclic voltammograms of $\mathbf{1}_H$ recorded in 50% (v/v) $CH_3CN-CH_2Cl_2$/0.1 M ($^nBu_4N$)(ClO_4) using a glassy-carbon working electrode at different scan rates.

of the octanuclear $[Cu_8(H)\{S_2CNH_2\}_6]^+$ model are given in Table 4. This model is found to adopt the $[Cu_4(\mu_4\text{-}H)Cu_4\{S_2CNH_2\}_6]^+$ tetracapped-tetrahedral (or triakis-tetrahedral)[23] geometry of T symmetry, in agreement with the X-ray structures of $\mathbf{1}_H$ and $\mathbf{2}_H$. In particular, there is a satisfying agreement between the computed $Cu_v-(\mu_4\text{-}H)$ distances (1.80 Å) and the corresponding experimental values of $\mathbf{1}_H$ and $\mathbf{2}_H$ (Table 1). The tetracapped tetrahedral geometry is found to be more stable than the perfect cubic one of T_h symmetry by 0.28 eV, the latter being not an energy minimum (several imaginary vibrational frequencies). On the other hand, the empty cluster $[Cu_8\{S_2CNH_2\}_6]^{2+}$ is found to adopt the cubic (T_h) geometry in the ground state (Table 4), as generally observed for this type of noncentered dithiolato octanuclear Cu(I) species,[44] including $[Cu_8\{S_2CN^nPr_2\}_6]^{2+}$.[24] These results are fully consistent with previous calculations on related isoelectronic dichalcogenophosphato octanuclear clusters.[21a,b] The NBO 1s population of the encapsulated hydride (1.69) is close to that found in the related dichalcogenophosphato species (~1.64), indicating rather similar covalent interactions resulting from an electron donation of the occupied 1s(hydride) AO into an in-phase combination of the vacant Cu^I sp_z orbitals. The bonding energy between H^- and the unrelaxed $[Cu_8\{S_2CNH_2\}_6]^{2+}$ fragment is equal to 11.31 eV and the energy lost by the empty $[Cu_8\{S_2CNH_2\}_6]^{2+}$ fragment when distorted from its T_h energy minimum to that which it adopts in $[Cu_4(\mu_4\text{-}H)Cu_4\{S_2CNH_2\}_6]^+$ is 0.69 eV. These values are comparable with those obtained in the dichalcogenophosphato series.[21a,b] The computed NMR chemical shift of the encapsulated hydride (7.6 ppm) is comparable to those observed for compounds $\mathbf{1}_H-\mathbf{3}_H$ (7.0–7.1 ppm).

The MO diagram of $[Cu_4(\mu_4\text{-}H)Cu_4\{S_2CNH_2\}_6]^+$ is shown in Figure 6, with the MO localizations listed. Most of the

dx.doi.org/10.1021/ic300135w | Inorg. Chem. 2012, 51, 6577–6591

Table 3. Photophysical Data for $[Cu_8(H)\{S_2CR\}_6](PF_6)$ (R = N^{n}Pr$_2$, $\mathbf{1_H}$; NEt$_2$, $\mathbf{2_H}$; aza-15-crown-5, $\mathbf{3_H}$)

compd	state (T/K)	λ^{ex}_{max} (nm)	λ^{em}_{max} (nm)	Stoke shift (cm^{-1})	λ^{ab}_{max} (nm) (ε/dm^3 mol^{-1} cm^{-1})	τ (μs)
$\mathbf{1_H}$	CH_2Cl_2 (77)	339–405	591	12 600	276 (68,000), 345 (37,000)	22, 4.6
	solid (77)	329, 445	576			
$\mathbf{2_H}$	CH_2Cl_2 (77)	335–411	596	13 100	276 (63,000), 350 (37,000)	20, 2.7
	solid (77)	330, 433	580			
$\mathbf{3_H}$	CH_2Cl_2 (77)	334–421	605	13 400	275 (66,000), 340 (35,000)	20, 4.4
	Solid (77)	325, 432	566			

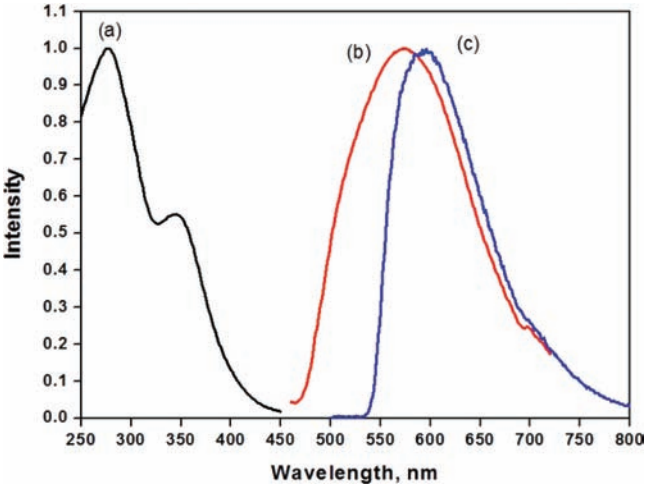

Figure 5. (a) UV–vis, (b) normalized emission spectra of compound **1** in the solid state at 77K, and (c) emission spectra of **1** in CH_2Cl_2 glass at 77 K.

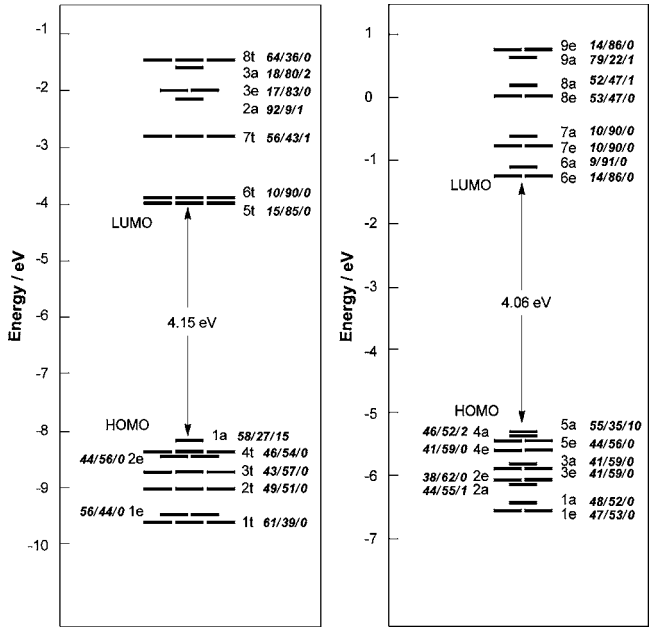

Figure 6. MO diagram of $[Cu_4(\mu_4\text{-H})(\mu_3\text{-Cu})_4\{S_2CNH_2\}_6]^+$ (left) and $Cu_4(\mu_4\text{-H})(\mu_3\text{-Cu})_3(S_2CNH_2)_6$ (right). The numerical values indicate the MO localization (%) in the following order: metals/ligands/μ_4-H.

highest occupied orbitals are of dominant ligand (mainly sulfur lone pairs) character, with significant 3d contributions of the eight copper atoms. The 1a HOMO is an exception with a metallic polarization (mainly dz^2 of the central tetrahedron) and some hydride admixture. The two lowest unoccupied levels can be viewed as the six combinations of the π^*(dtc) ligands. Above these two levels, one finds orbitals with dominant Cu character. The lowest UV–vis optical transitions have been calculated at the TDDFT level, and the corresponding simulated absorption spectrum is shown in the middle of Figure 7 (see Computational Details). With a simulated low energy band at λ_{max} = 326 nm and a more intense band at λ_{max} = 264 nm, it fits quite well with the recorded experimental spectra of $\mathbf{1_H}$, $\mathbf{2_H}$, and $\mathbf{3_H}$ (λ_{max} = 325–335 nm and λ_{max} ~ 270 nm; see Table 3 and Figure 5a). The low energy band is associated with MLCT transitions, as exemplified by its major component computed at 335 nm which corresponds to the 4t → 6t transition. Almost all the transitions contributing to the band at λ_{max} = 264 nm are also of the MLCT type, although its major component at 282 nm corresponds to the 1a → 7t transition which is primarily hydride to ligand in character. Interestingly, the simulated absorption spectrum of the empty T_h cluster $[Cu_8\{S_2CNH_2\}_6]^{2+}$ (left side of Figure 7) exhibits a

Table 4. Relevant Computed Data for $[Cu_8(S_2CNH_2)_6]^{2+}$, $[Cu_4(\mu_4\text{-H})Cu_4\{S_2CNH_2\}_6]^+$, $[Cu_7\{S_2CNH_2\}_6]^+$, and $Cu_4(\mu_4\text{-H})Cu_3\{S_2CNH_2\}_6$ in Their Equilibrium Geometries

	$[Cu_8(S_2CNH_2)_6]^{2+}$ S = 0	$[Cu_4(\mu_4\text{-H})(\mu_3\text{-Cu})_4\{S_2CNH_2\}_6]^+$ S = 0	$[Cu_4(\mu_4\text{-H})(\mu_3\text{-Cu})_4\{S_2CNH_2\}_6]^+$ S = 1	$[Cu_7(S_2CNH_2)_6]^+$ S = 0	$Cu_4(\mu_4\text{-H})(\mu_3\text{-Cu})_3\{S_2CNH_2\}_6$ S = 0
symmetry	T_h	T	C_2	C_3	C_3
HOMO–LUMO gap/ eV	3.91	4.15		3.88	4.06
Cu_v–H/Å		1.800 × 4	(1.812, 1.844) × 2		1.778 × 3, 1.846
Cu_v–Cu_v/Å	2.841 × 12	2.939 × 6	2.833–3.026 (range)	(2.829, 2.746, 3.012) × 3	(2.763, 3.078) × 3
Cu_v–Cu_{cap}/Å		2.634 × 12	2.597–2.755 (range)		(2.643, 2.630, 2.612) × 3
Cu_v–S/Å	2.286 × 4	2.402 × 12	2.259–2.481 (range)	2.253–2.306 (range)	2.376–2.593 (range)
Cu_{cap}–S/Å		2.306 × 12	2.259–2.318 (range)		2.286–2.327 (range)
S···S (bite)/ Å	3.091 × 6	3.081 × 6	3.073–3.100 (range)	3.078–3.088 (range)	3.056–3.071 (range)
μ_4-H NBO charges		−0.69			−0.68
NMR chemical shift of μ_4-H		7.6			6.5

dx.doi.org/10.1021/ic300135w | Inorg. Chem. 2012, 51, 6577–6591

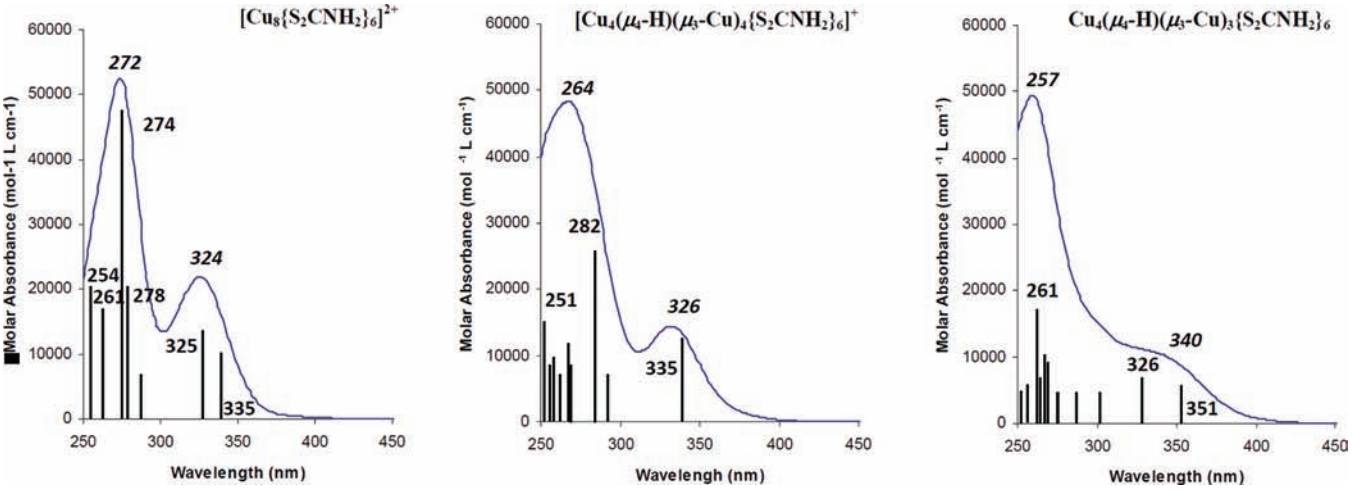

Figure 7. Simulated absorption spectra of the models $[Cu_8\{S_2CNH_2\}_6]^{2+}$ (left), $[Cu_4(\mu_4\text{-H})(\mu_3\text{-Cu})_3(S_2CNH_2)_6]^+$ (middle), and $Cu_4(\mu_4\text{-H})(\mu_3\text{-Cu})_3(S_2CNH_2)_6$ (right). Solid lines represent the calculated transitions, and their lengths are proportional to their oscillator strengths (os). Only transitions with os >0.02 are shown. Values in italics indicate the theoretical λ_{max} values on the simulated curves.

very similar peak profile as that of $[Cu_4(\mu_4\text{-H})\text{-}Cu_4\{S_2CNH_2\}_6]^+$, with a low-energy band at λ_{max} = 325 nm and an intense high-energy band at λ_{max} = 274 nm. Most of the transitions associated with these bands are also of the MLCT type. This result matches the interpretation of the spectral changes shown in Figure 3.

The optimized geometry of the lowest triplet state of $[Cu_8(H)\{S_2CNH_2\}_6]^+$ adopts a distorted tetracapped tetrahedral geometry of C_2 symmetry (Table 4). It lies 2.93 eV above the singlet ground state. The emission wavelength of the cluster has been calculated as the difference between the energy of the optimized triplet state and that of the singlet state assuming the same (unrelaxed) geometry as that of the triplet state. The corresponding value (506 nm) compares reasonably well with the corresponding experimental data recorded in the solid state for $\mathbf{1_H}$, $\mathbf{2_H}$, and $\mathbf{3_H}$ (~570−580 nm; see Table 3). When PCM solvent (CH_2Cl_2) corrections are considered,[45] the computed transition shifts to 655 nm, whereas the corresponding experimental values are close to 600 nm (Table 3).

$[Cu_7(H)\{S_2CNH_2\}_6]$. The optimized geometry of $Cu_7(H)\text{-}(S_2CNH_2)_6$ (Table 4) was found to adopt a $Cu_4(\mu_4\text{-}H)Cu_3(S_2CNH_2)_6$ tricapped-tetrahedral geometry of C_3 symmetry. Interestingly, it differs from the X-ray and neutron structure of $\mathbf{6_H}$ in that the central $(Cu_v)_4$ tetrahedron is only moderately elongated along the C_3 axis, with an elongated edge of 3.08 compared to 3.38 Å (av.) as determined in the X-ray diffraction study of $\mathbf{6_H}$. More importantly, the Cu6 atom is not bonded to two sulfur atoms as revealed in the crystal structure of $\mathbf{6_H}$ (Figure 2), but to three of them, just like Cu2 and Cu4, these three metals being symmetry related in C_3 symmetry. It should be noted that calculations commenced from geometry derived from the experimental structure of $\mathbf{6_H}$ ended up at the unique C_3 energy minimum. We attribute this difference between $[Cu_7(\mu_4\text{-H})\{S_2CNH_2\}_6]$ and $\mathbf{6_H}$ to the presence of bulky aza-crown-5 substituents in $\mathbf{6_H}$, which presumably induce steric and packing distortions in the solid state. This is supported by the fact that related isoelectronic heptanuclear dicalcogenophosphato silver(I) clusters adopt the same structure as our computed model.[46] Thus, the structure of $[Cu_4(\mu_4\text{-H})Cu_3\{S_2CNH_2\}_6]$ can be described as resulting from the removal of one capping Cu^I ion from $[Cu_4(\mu_4\text{-H})\text{-}Cu_4\{S_2CNH_2\}_6]^+$. Apart from this removal, both clusters have similar connectivities. In particular, the encapsulated hydride of $[Cu_7(\mu_4\text{-H})\{S_2CNH_2\}_6]$ is found to lie in the middle of the elongated central tetrahedron with Cu−H distances of 1.78 and 1.85 Å. The Cu_{cap}−H distance (2.52 Å) is rather long, thus the hydride is clearly tetrahedrally coordinated, as demonstrated in the neutron structure of $\mathbf{6_H}$. The computed NMR chemical shift of the encapsulated hydride (6.5 ppm) is in excellent agreement with those observed for compounds $\mathbf{4_H}$−$\mathbf{6_H}$ (6.5−6.6 ppm).

Interestingly, the hypothetical empty cluster $[Cu_7\{S_2CNH_2\}_6]^+$ does not retain the tricapped tetrahedral arrangement of the copper framework in its equilibrium geometry, but rather relaxes to a structure of C_3 symmetry which can be approximated to a cube having one vacant vertex, i.e., deriving from that of $[Cu_8\{S_2CNH_2\}_6]^{2+}$ by the removal of one Cu^+ ion. Thus, the tetrahedral distortion afforded by the metal atoms in the hydrido clusters is attributed to a hydride template effect, both in the hepta- and octanuclear species.

The bonding energy between the encapsulated hydride and the unrelaxed $[Cu_7\{S_2CNH_2\}_6]^+$ fragment is equal to 8.45 eV, whereas the energy lost by the empty $[Cu_7\{S_2CNH_2\}_6]^+$ fragment when distorted from its equilibrium geometry to that it adopts in $[Cu_4(\mu_4\text{-H})Cu_3\{S_2CNH_2\}_6]$ is 0.80 eV. The bonding energy is lower than that found in $[Cu_8(\mu_4\text{-}H)\{S_2CNH_2\}_6]^+$ (vide supra) whereas the NBO 1s(μ_4-H) population (1.68) is almost equal to that found in the octanuclear parent. These results indicate similar strengths for the covalent bonding of H^- in $[Cu_4(\mu_4\text{-H})Cu_3\{S_2CNH_2\}_6]$ and $[Cu_4(\mu_4\text{-H})Cu_4\{S_2CNH_2\}_6]^+$, but weaker ionic bonding in the former, consistent with the lower charge of the hosting cage. The MO diagram of $[Cu_7(\mu_4\text{-H})\{S_2CNH_2\}_6]$ is shown in Figure 6, with the major MO localizations listed. Its frontier orbitals exhibit very similar characteristics as its octanuclear relative (vide supra). Its absorption spectrum has also been simulated from TDDFT calculations (see the right side of Figure 7). It exhibits a similar shape to its octanuclear relative, with a low energy MLCT absorption band around 340 nm and a more intense band around 247 nm, both of them being largely of the MLCT type.

$[Cu^{II}(S_2CNH_2)_2]$. In order to confirm the interpretation of the absorption spectral changes mentioned above and shown in Figure 3, the optical transitions of $[Cu^{II}(S_2CNH_2)_2]$ have also

dx.doi.org/10.1021/ic300135w | Inorg. Chem. 2012, 51, 6577−6591

been computed at the TDDFT level on its equilibrium geometry which was found to adopt a planar D_{2h} geometry. A strong optical LMCT transition (oscillator strength = 0.248 nm) is computed at 416 nm, whereas a HOMO-2 → LUMO symmetry forbidden LMCT transition is found at 647 nm, the latter being experimentally observable in the $[Cu^{II}(S_2CNR_2)_2]$ (R ≠ H) complexes due to the lower symmetry induced by the R group. These results fully agree with the indexing to the $[Cu^{II}(SCR_2)_2]$ species which displays two bands of lowest energy in Figure 3.

CONCLUSION

The synthesis of hydride-centered tetracapped-tetrahedral Cu_8 clusters surrounded by six 1,1-dichalcogenolate ligands has been successfully extended to utilize dithiocarbamates as the supporting ligands. Exploiting the redox-tolerant nature, which is not a feature of dichalcogenophosphates, the encapsulated hydride in compounds **1**−**3** can be oxidatively released via the reaction of $[Ce(NO_3)_6]^{2-}$ to afford $[Cu^{II}(dtc)_2]$ and Cu^{I} salts. Reactions of $[Cu^{II}(dtc)_2]$ and Cu^{I} in the presence of borohydride in solution reproduce clusters **1**−**3** which can be monitored by the UV−vis titration experiments.

Reactions of 1 equiv of borohydride with Cu_8 clusters **1**−**3** produce neutral, heptanuclear copper clusters, **4**−**6**, with a copper framework which is a tricapped triangular pyramid in which the hydride occupies a central tetrahedral site. The four-coordinate hydride within the Cu_7 cluster is unequivocally authenticated by neutron diffraction analysis performed on a single crystal of **6**. The reactions of Cu^{I} ion with hydride-centered Cu_7 clusters in solution reproduce clusters **1**−**3** in quantitative yield. In addition, the clusters **4**−**6** can be directly synthesized from Cu^{II} salts, dithiocarbamates, and borohydrides in a 7:6:8 molar ratio. Compounds **1**−**6** are air stable.

DFT calculations on model compounds fully reproduce the experimental structures of the Cu_8H and Cu_7H species, including the position of the hydride in the middle of the central tetrahedron. The difference in the hydride chemical shifts between the two species was matched by DFT. The UV−vis absorption spectra of the studied compounds have been indexed through TDDFT modeling and the luminescent nature of **1**−**3** has been shown to be associated with a ^{3}MLCT excited state.

EXPERIMENTAL SECTION

Reagents and General Procedures. All chemicals were purchased from commercial sources and used as received. Solvents were purified following standard protocols. All reactions were performed in oven-dried Schlenk glassware using standard inert-atmosphere techniques. All reactions were carried out under N_2 atmosphere by using standard Schlenk techniques. The preparation of $[Cu(CH_3CN)_4](PF_6)$[47] and the $Na(S_2CR)$ ligands (R = N^nPr_2, NEt_2, and aza-15-crown-5) have been reported previously.[48] The syntheses of $Cu^{II}(S_2CR)_2$ (R = N^nPr_2, NEt_2, and aza-15-crown-5) have also been described.[40] Melting points were measured by using a Fargo MP-2D melting point apparatus. The elemental analyses were done using a Perkin-Elmer 2400 CHN analyzer.

Spectroscopic Methods. NMR spectra were recorded on Bruker Advance DPX300 FT-NMR spectrometer that operates at 300 MHz while recording ^{1}H, 121.5 MHz for ^{31}P, and 46.1 MHz for ^{2}H. The $^{31}P\{^1H\}$ NMR are referenced externally against 85% H_3PO_4 (δ = 0 ppm). The chemical shift (δ) and coupling constant (J) are reported in parts per million and hertz. The NMR spectra were recorded at ambient temperature. ESI-mass spectra were recorded on a Fison Quattro Bio-Q (Fisons Instruments, VG Biotech, UK). UV−visible absorption spectra were measured on a Perkin-Elmer Lambda 750 spectrophotometer using quartz cells with path length of 1 cm recording in the 250−750 nm region. The cyclic voltammograms were recorded on a CH Instruments 611C electrochemical analyzer using a glassy carbon working electrode, Pt wire auxiliary electrode, Ag/$AgNO_3$ reference electrode (0.33 V ± 10 mV versus SCE), and standardized by the redox couple ferricinium/ferrocene. $(Bu_4N)(ClO_4)$ (0.1 M) was used as the supporting electrolyte, and 50% (v/v) $CH_3CN-CH_2Cl_2$ solution was used for all of the samples. Electrochemical solutions were degassed with N_2 and maintained under a positive pressure for the duration of the experiment. All infrared spectra were recorded on a Bruker Optics FTIR TENSOR 27 spectrometer at 20 °C using CsI plate. GC/MS analyses were carried out on a Finnigan trace GC to which a Finnigan trace mass selective detector was attached. The GC was equipped with an EQUITY-5 fused silica capillary column (30 m × 0.25 mm ×0.25 μm film thickness). Helium was used as carrier gas and the following temperature program was employed: initial isothermal period of 1 min at 35 °C, then an increase at 1 °C/min to 50 °C with an isothermal period of 15 min at 50 °C. Emission spectra were recorded on a Cary Eclipse B10 fluorescence spectrophotometer. The 77 K emission lifetimes determined by a scope system at Fu-Jen Catholic University used a PTI's Model GL302 Dye Laser pumping by GL-3300 Nitrogen Laser for excitation and a Hamamatsu P9220 PMT/E717-63 socket assembly mounted on a Jobin-Yvon H-100 spectrometer for detection. Photomultiplier (PMT) output was digitized using LeCory WaveRunner 6030A, 350 MHz normal analog bandwidth, 2.5 GS/s single-shot sample rate/Ch, acquisition Memory 2 MB/4 MB for 4 ch/2 ch. Solid samples were prepared in capillary for lifetime studies, and the 77 K emission lifetimes determined used samples in 2 mm cylindrical cells immersed in liquid N_2 in a Dewar as previously described.[49]

Monitoring of the Hydride Abstraction and Cluster Reformation by UV−vis. Both forward and backtitration experiments were monitored by UV−vis. Compound **1** in 50% (v/v) $CH_3CN-CH_2Cl_2$ solution (2 mL, 6.6×10^{-5} M) was added into the quartz cells (3.5 mL, 1 cm) before determination. The titrants including both oxidizer $(NH_4)_2[Ce(NO_3)_6]$ (4.4×10^{-4} M) and reductant, $(Bu_4N)(BH_4)$ (4.4×10^{-4} M) were prepared with 50% (v/v) $CH_3CN-CH_2Cl_2$ solution, and 0.33 equiv (0.1 mL) of oxidizer and/or reductant were stepwise added to the sample solution each time.

Synthesis: $[Cu_4(\mu_4\text{-}H)(\mu_3\text{-}Cu)_4\{S_2CN^nPr_2\}_6](PF_6)$, $\mathbf{1_H}$. *Method A.* $[Cu(CH_3CN)_4](PF_6)$ (0.50 g, 1.338 mmol), $Na(S_2CN^nPr_2)$ (0.20 g, 1.003 mmol), and $(Bu_4N)(BH_4)$ (0.043 g, 0.167 mmol) in 30 mL of CH_3CN were added to a Schlenk flask (100 mL) and were stirred at room temperature for 1 h under nitrogen atmosphere. The reaction mixture was evaporated to dryness under vacuum to obtain a yellow solid. The yellow solid was added to 30 mL of $CHCl_3$ to form a yellow solution, and the solution was washed with deionized water (3 × 20 mL). The solution was filtered and the filtrate was evaporated to dryness under vacuum to yield complex $\mathbf{1_H}$ as a yellow powder. Yield: 0.223 g (78%).

Method B. $Cu^{II}(S_2CN^nPr_2)_2$ (0.30 g, 0.720 mmol), $[Cu(CH_3CN)_4](PF_6)$ (0.447 g, 1.20 mmol), and $(Bu_4N)(BH_4)$ (0.247 g, 0.960 mmol) in 30 mL CH_3CN were added to a 100 mL Schlenk flask and stirred at room temperature for 10 min under nitrogen atmosphere. The reaction mixture was evaporated to dryness under vacuum to obtain a yellow solid. The solid was washed with deionized water (3 × 20 mL) and dried under vacuum to give complex $\mathbf{1_H}$ as a yellow powder. Yield: 0.292 g (71%). Mp: 249 °C (dec). Anal. Calcd for $Cu_8H_{85}C_{42}N_6PF_6S_{12}\cdot 0.5CH_3CN$: C, 29.80; H, 5.03; N, 5.25%. Found: C, 29.95; H, 5.15; N, 5.19%. ^{1}H NMR (300 MHz, $CDCl_3$, δ, ppm): 7.05 (bs, 1H, μ_4-H), 0.95 (t, $^3J_{HH}$ = 7.3 Hz, 36H, $CH_2CH_2CH_3$), 1.83 (m, 24H, $CH_2CH_2CH_3$), 3.99 (t, $^3J_{HH}$ = 7.7 Hz, 24H, $CH_2CH_2CH_3$). ^{31}P NMR ($CDCl_3$): −143.0 (septet, $^1J_{PF}$ = 706.2 Hz, PF_6). ESI-MS (m/z)(Cal.): 1568.1 (1567.31) $[Cu_8(H)\{S_2CN^nPr_2\}_6]^+$. UV−vis [$\lambda_{max}$ in nm, (ε in M^{-1} cm^{-1})], 276(68 000), 345(37 000). IR (CsI, cm^{-1}): ν(Cu−S), 233; ν(S−C), 944; ν(C−N), 1501, $\nu(PF_6^-)$, 843.

dx.doi.org/10.1021/ic300135w | Inorg. Chem. 2012, 51, 6577−6591

$[Cu_4(\mu_4\text{-}D)(\mu_3\text{-}Cu)_4\{S_2CN^nPr_2\}_6](PF_6)$. $\mathbf{1_D}$ was prepared in a similar fashion to $\mathbf{1_H}$ by replacing $(Bu_4N)(BH_4)$ with $(Bu_4N)(BD_4)$. Yield: 0.209 g (73%). Mp: 253 °C (dec). Anal. Calcd for $Cu_8H_{84}DC_{42}N_6PF_6S_{12} \cdot 1.5CHCl_3$: C, 27.61; H, 4.66; N, 4.44%. Found: C, 27.52; H, 4.99; N, 4.39%. ^{1}H NMR (300 MHz, $CDCl_3$, δ, ppm): 0.94 (t, $^3J_{HH}$ = 7.3 Hz, 36H, $CH_2CH_2CH_3$), 1.82 (m, 24H, $CH_2CH_2CH_3$), 3.98 (t, $^3J_{HH}$ = 7.7 Hz, 24H, $CH_2CH_2CH_3$). ^{2}H NMR (46.1 MHz, $CDCl_3$, δ, ppm): 7.07 (bs, 1D). ^{31}P NMR ($CDCl_3$): −143.0 (septet, $^1J_{PF}$ = 706.1 Hz, PF_6). ESI-MS (m/z)(Cal.): 1569.2 (1568.32) $[Cu_8(D)\{S_2CN^nPr_2\}_6]^+$. UV−vis [$\lambda_{max}$ in nm, (ε in $M^{-1}cm^{-1}$)], 275(67 000), 345(37 000). IR (CsI, cm^{-1}): ν(Cu−S), 233; ν(S−C), 943; ν(C−N), 1501, $\nu(PF_6^-)$, 843.

$[Cu_4(\mu_4\text{-}H)(\mu_3\text{-}Cu)_4\{S_2CNEt_2\}_6](PF_6)$. $\mathbf{2_H}$ was synthesized in a similar procedure to $\mathbf{1_H}$ using $Na(S_2CNEt_2)$ instead of $Na(S_2CN^nPr_2)$. Yield: 0.195 g (65%). Mp: 238 °C (dec). Anal. Calcd for $Cu_8H_{61}C_{30}N_6PF_6S_{12}$: C, 23.34; H, 3.98; N, 5.44%. Found: C, 23.24; H, 4.14; N, 5.64%. ^{1}H NMR (300 MHz, CD_2Cl_2, δ, ppm): 7.02 (bs, 1H, μ_4-H), 1.31 (t, $^3J_{HH}$ = 7.4 Hz, 24H, CH_2CH_3), 4.05 (m, $^3J_{HH}$ = 7.4 Hz, 36H, CH_2CH_3). ^{31}P NMR ($CDCl_3$): −143.0 (septet, $^1J_{PF}$ = 706.1 Hz, PF_6). ESI-MS (m/z)(Cal.): 1400.8 (1398.99) $[Cu_8(H)\{S_2CNEt_2\}_6]^+$. UV−vis [$\lambda_{max}$ in nm, (ε in M^{-1} cm^{-1})], 276(63 000), 350(37 000). IR (CsI, cm^{-1}): ν(Cu−S), 230; ν(S−C), 970; ν(C−N), 1505, $\nu(PF_6^-)$, 843.

$[Cu_4(\mu_4\text{-}D)(\mu_3\text{-}Cu)_4\{S_2CNEt_2\}_6](PF_6)$. $\mathbf{2_D}$ was prepared in a similar fashion to $\mathbf{2_H}$ by replacing $(Bu_4N)(BH_4)$ with $(Bu_4N)(BD_4)$. Yield: 0.208 g (69%). Mp: 246 °C (dec). Anal. Calcd for $Cu_8H_{60}DC_{30}N_6PF_6S_{12}$: C, 23.32; H, 4.04; N, 5.44%. Found: C, 23.65; H, 4.04%; N, 5.19%. ^{1}H NMR (300 MHz, CD_2Cl_2, δ, ppm): 1.30 (t, $^3J_{HH}$ = 7.0 Hz, 24H, CH_2CH_3), 4.05 (m, $^3J_{HH}$ = 7.0 Hz, 36H, CH_2CH_3). ^{2}H NMR (46.1 MHz, CD_2Cl_2, δ, ppm): 7.02 (bs, 1D). ^{31}P NMR ($CDCl_3$): −143.0 (septet, $^1J_{PF}$ = 706.0 Hz, PF_6). ESI-MS (m/z)(Cal.): 1402.5 (1400.00) $[Cu_8(D)\{S_2CNEt_2\}_6]^+$. UV−vis [$\lambda_{max}$ in nm, (ε in M^{-1} cm^{-1})], 276(63 000), 353(37 000). IR (CsI, cm^{-1}): ν(Cu−S), 231; ν(S−C), 970; ν(C−N), 1505, $\nu(PF_6^-)$, 843.

$[Cu_4(\mu_4\text{-}H)(\mu_3\text{-}Cu)_4\{S_2C(aza\text{-}15\text{-}crown\text{-}5)\}_6](PF_6)$. $\mathbf{3_H}$ was similarly synthesized as described for $\mathbf{1_H}$ using (Na)[S_2C(aza-15-crown-5)] instead of $Na(S_2CN^nPr_2)$. Yield: 0.147 g (77%). Mp: 246 °C (dec). Anal. Calcd for $Cu_8H_{121}C_{66}N_6PF_6O_{24}S_{12}\cdot 0.5(CH_3)_2CO$: C, 33.09; H, 5.10; N, 3.43%. Found: C, 33.17; H, 5.06; N, 3.64%. ^{1}H NMR (300 MHz, $CDCl_3$, δ, ppm): 7.03 (bs, 1H, μ_4-H), 4.40 (t, $^3J_{HH}$ = 5.8 Hz, 24H, NCH_2CH_2O), 3.93 (t, $^3J_{HH}$ = 6.0 Hz, 24H, NCH_2CH_2O), 3.64 (m, 72H, OCH_2CH_2O). ^{31}P NMR ($CDCl_3$): −143.0 (septet, $^1J_{PF}$ = 706.0 Hz, PF_6). ESI-MS (m/z)(Cal.): 2275.4 (2275.84) $[Cu_8(H)\{S_2CNC_{10}H_{20}O_4\}_6]^+$. UV−vis [$\lambda_{max}$ in nm, (ε in M^{-1} cm^{-1})], 275(66 000), 340(35 000). IR (CsI, cm^{-1}): ν(Cu−S), 233; ν(S−C), 991; ν(C−N), 1490, $\nu(PF_6^-)$, 843.

$[Cu_4(\mu_4\text{-}D)(\mu_3\text{-}Cu)_4\{S_2C(aza\text{-}15\text{-}crown\text{-}5)\}_6](PF_6)$. $\mathbf{3_D}$ was prepared in a similar fashion to $\mathbf{3_H}$ by replacing $(Bu_4N)(BH_4)$ with $(Bu_4N)(BD_4)$. Yield: 0.137 g (72%). Mp: 247 °C (dec). Anal. Calcd for $Cu_8H_{120}D_1C_{66}N_6PF_6O_{24}S_{12}\cdot 1(CH_3)_2CO$: C, 33.42; H, 5.20; N, 3.39%. Found: C, 33.37; H, 5.25; N, 3.45%. ^{1}H NMR (300 MHz, $CDCl_3$, δ, ppm): 4.41 (t, $^3J_{HH}$ = 5.8 Hz, 24H, NCH_2CH_2O), 3.93 (t, $^3J_{HH}$ = 6.0 Hz, 24H, NCH_2CH_2O), 3.66 (m, 72H, OCH_2CH_2O). ^{2}H NMR (300 MHz, $CDCl_3$, δ, ppm): 7.02 (bs, 1D). ^{31}P NMR ($CDCl_3$): −143.0 (septet, $^1J_{PF}$ = 706.0 Hz, PF_6). ESI-MS (m/z)(Cal.): 2276.7 (2276.85) $[Cu_8(D)\{S_2CNC_{10}H_{20}O_4\}_6]^+$. UV−vis [$\lambda_{max}$ in nm, (ε in M^{-1} cm^{-1})], 276(66 000), 341(35 000). IR (CsI, cm^{-1}): ν(Cu−S), 233; ν(S−C), 990; ν(C−N), 1490, $\nu(PF_6^-)$, 843.

$[Cu_4(\mu_4\text{-}H)(\mu_3\text{-}Cu)_3\{S_2CN^nPr_2\}_6]$, $\mathbf{4_H}$. *Method A.* To a dichloromethane solution (20 mL) of $[Cu_4(\mu_4\text{-}H)(\mu_3\text{-}Cu)_4\{S_2CN^nPr_2\}_6](PF_6)$ (0.171 g, 0.1 mmol) was added $(Bu_4N)(BH_4)$ (0.026 g, 0.1 mmol). The solution color changed from yellow to red-brown after 1 h of stirring, after which the solution was filtered through Al_2O_3 to remove copper particles then evaporated to dryness under vacuum. The crude product was washed with ethanol (3 × 5 mL), and then the solid was dried under vacuum to obtain complex $\mathbf{4_H}$ as yellow powder. Yield: 0.123 g (82%).

Method B. $Cu(BF_4)_2$ (0.278 g, 1.171 mmol), $Na(S_2CN^nPr_2)_2$ (0.20 g, 1.003 mmol), and $(Bu_4N)(BH_4)$ (0.344 g, 1.337 mmol) were charged in a 100 mL Schlenk flask. A total of 30 mL of CH_3CN was added to it and stirred at room temperature for 10 min. The reaction mixture was evaporated to dryness under vacuum to obtain a yellow solid. The solid was washed with ethanol (3 × 5 mL), and then dried under vacuum to obtain complex $\mathbf{4_H}$ as yellow powder. Yield: 0.189 g (75%). Mp: 154 °C (dec). Anal. Calcd for $Cu_7H_{85}C_{42}N_6S_{12}\cdot 0.5CH_2Cl_2$: C, 33.01; H, 5.61; N, 5.44%. Found: C, 32.99; H, 5.98; N, 5.22%. ^{1}H NMR (300 MHz, $CDCl_3$, δ, ppm): 6.55 (bs, 1H, μ_4-H), 0.88 (t, $^3J_{HH}$ = 7.4 Hz, 36H, $CH_2CH_2CH_3$), 1.78 (m, 24H, $CH_2CH_2CH_3$), 3.90 (t, $^3J_{HH}$ = 7.8 Hz, 24H, $CH_2CH_2CH_3$). UV−vis [λ_{max} in nm, (ε in M^{-1} cm^{-1})], 274(65 000), 352(34 000). IR (CsI, cm^{-1}): ν(Cu−S), 201; ν(S−C), 959; ν(C−N), 1484.

$[Cu_4(\mu_4\text{-}D)(\mu_3\text{-}Cu)_3\{S_2CN^nPr_2\}_6]$. $\mathbf{4_D}$ was prepared as for $\mathbf{4_H}$ by replacing $(Bu_4N)(BH_4)$ with $(Bu_4N)(BD_4)$. Yield: 0.128 g (85%). Mp: 159 °C (dec). Anal. Calcd for $Cu_7H_{84}D_1C_{42}N_6S_{12}\cdot 2CH_2Cl_2$: C, 31.56; H, 5.42; N, 5.02%. Found: C, 31.49; H, 5.67; N, 4.54%. ^{1}H NMR (300 MHz, $CDCl_3$, δ, ppm): 0.88 (t, $^3J_{HH}$ = 7.3 Hz, 36H, $CH_2CH_2CH_3$), 1.77 (m, 24H, $CH_2CH_2CH_3$), 3.91 (t, $^3J_{HH}$ = 7.7 Hz, 24H, $CH_2CH_2CH_3$). ^{2}H NMR (46.1 MHz, $CDCl_3$, δ, ppm): 6.40 (bs, 1D). UV−vis [λ_{max} in nm, (ε in M^{-1} cm^{-1})], 273(65 000), 352(34 000). IR (CsI, cm^{-1}): ν(Cu−S), 202; ν(S−C), 960; ν(C−N), 1485.

$[Cu_4(\mu_4\text{-}H)(\mu_3\text{-}Cu)_3\{S_2CNEt_2\}_6]$. $\mathbf{5_H}$ was synthesized as described for $\mathbf{4_H}$ by using $[Cu_4(\mu_4\text{-}H)(\mu_3\text{-}Cu)_4\{S_2CNEt_2\}_6](PF_6)$ instead of $[Cu_4(\mu_4\text{-}H)(\mu_3\text{-}Cu)_4\{S_2CN^nPr_2\}_6](PF_6)$. Yield: 0.106 g (79%). Mp: 137 °C (dec). Anal. Calcd for $Cu_7H_{61}C_{30}N_6S_{12}\cdot 2H_2O$: C, 26.27; H, 4.78; N, 6.13%. Found: C, 26.26; H, 4.91; N, 5.90%. ^{1}H NMR (300 MHz, CD_2Cl_2, δ, ppm): 6.55 (bs, 1H, μ_4-H), 1.31 (t, $^3J_{HH}$ = 7.3 Hz, 24H, CH_2CH_3), 4.04 (m, $^3J_{HH}$ = 8.4 Hz, 36H, CH_2CH_3). UV−vis [λ_{max} in nm, (ε in M^{-1} cm^{-1})], 275(64 000), 353(37 000). IR (CsI, cm^{-1}): ν(Cu−S), 210; ν(S−C), 978; ν(C−N), 1489.

$[Cu_4(\mu_4\text{-}D)(\mu_3\text{-}Cu)_3\{S_2CNEt_2\}_6]$. $\mathbf{5_D}$ was prepared in a similar fashion to $\mathbf{5_H}$ by replacing $(Bu_4N)(BH_4)$ with $(Bu_4N)(BD_4)$. Yield: 0.109 g (81%). Mp: 142 °C (dec). Anal. Calcd for $Cu_7H_{60}DC_{30}N_6S_{12}\cdot 1.5CH_2Cl_2$: C, 25.85; H, 4.48; N, 5.74%. Found: C, 25.78; H, 4.80; N, 5.59%. ^{1}H NMR (300 MHz, CD_2Cl_2, δ, ppm): 1.30 (t, $^3J_{HH}$ = 7.3 Hz, 24H, CH_2CH_3), 4.04 (m, $^3J_{HH}$ = 8.4 Hz, 36H, CH_2CH_3). ^{2}H NMR (300 MHz, CD_2Cl_2, δ, ppm): 6.50 (bs, 1D). UV−vis [λ_{max} in nm, (ε in M^{-1} cm^{-1})], 276(64 000), 351(37 000). IR (CsI, cm^{-1}): ν(Cu−S), 208; ν(S−C), 978; ν(C−N), 1490.

$[Cu_4(\mu_4\text{-}H)(\mu_3\text{-}Cu)_3\{S_2C(aza\text{-}15\text{-}crown\text{-}5)\}_6]$. $\mathbf{6_H}$ was synthesized as described for $\mathbf{4_H}$ by using $[Cu_4(\mu_4\text{-}H)(\mu_3\text{-}Cu)_4\{S_2CN(aza\text{-}15\text{-}crown\text{-}5)\}_6](PF_6)$ instead of $[Cu_4(\mu_4\text{-}H)(\mu_3\text{-}Cu)_4\{S_2CN^nPr_2\}_6]$ (PF_6). Yield: 0.097 g (87%). Mp: 217 °C (dec). Anal. Calcd for $Cu_7H_{121}C_{66}N_6O_{24}S_{12}$: C, 35.83; H, 5.51; N, 3.80%. Found: C, 35.80; H, 5.39; N, 3.61%. ^{1}H NMR (300 MHz, $CDCl_3$, δ, ppm): 6.49 (bs, 1H, μ_4-H), 4.28 (t, $^3J_{HH}$ = 5.4 Hz, 24H, NCH_2CH_2O), 3.92 (t, $^3J_{HH}$ = 5.7 Hz, 24H, NCH_2CH_2O), 3.64 (m, 72H, OCH_2CH_2O). UV−vis [λ_{max} in nm, (ε in M^{-1} cm^{-1})], 275(64 000), 340(36 000). IR (CsI, cm^{-1}): ν(Cu−S), 201; ν(S−C), 988; ν(C−N), 1483.

$[Cu_4(\mu_4\text{-}D)(\mu_3\text{-}Cu)_3\{S_2C(aza\text{-}15\text{-}crown\text{-}5)\}_6]$. $\mathbf{6_D}$ was prepared as for $\mathbf{6_H}$ by replacing $(Bu_4N)(BH_4)$ with $(Bu_4N)(BD_4)$. Yield: 0.094 g (85%). Mp: 220 °C (dec). Anal. Calcd for $Cu_7H_{120}D_1C_{66}N_6O_{24}S_{12}$: C, 35.82; H, 5.56; N, 3.80%. Found: C, 35.78; H, 5.34; N, 3.69%. ^{1}H NMR (300 MHz, $CDCl_3$, δ, ppm): 4.30 (t, $^3J_{HH}$ = 5.8 Hz, 24H, NCH_2CH_2O), 3.93 (t, $^3J_{HH}$ = 6.0 Hz, 24H, NCH_2CH_2O), 3.64 (m, 72H, OCH_2CH_2O). ^{2}H NMR (300 MHz, $CDCl_3$, δ, ppm): 6.51 (bs, 1D). UV−vis [λ_{max} in nm, (ε in M^{-1} cm^{-1})], 275(64 000), 340(36 000). IR (CsI, cm^{-1}): ν(Cu−S), 202; ν(S−C), 988; ν(C−N), 1485.

$[Cu\{S_2C(aza\text{-}15\text{-}crown\text{-}5)\}_2]$, 7. A synthesis of compound 7 has been reported,[40] but here we present a new synthesis. To a 50% (v/v) CH_3CN−CH_2Cl_2 solution of compound $\mathbf{3_H}$ (0.10 g, 0.041 mmol), $(NH_4)_2[Ce(NO_3)_6]$ (0.091 g, 0.164 mmol) was added. The yellow solution turned brown rapidly, and the resulting brown solution was stirred for about 1 h. The solution was filtered to remove any solid, and the filtrate was evaporated to dryness to give a dark-brown powder. This was washed with deionized water (5 × 5 mL) and dried under vacuum to obtain complex 7 as brown powder. Yield: 0.054 g (67%). Mp: 165 °C. Anal. Calcd for $Cu_1H_{40}C_{22}N_2O_8S_4\cdot 1.5H_2O$: C, 39.95; H, 6.25; N, 4.24%. Found: C, 39.99; H, 5.95; N, 4.08%. UV−vis [λ_{max} in nm, (ε in M^{-1} cm^{-1})], 271(30 000), 434(14 000), 600(1000). IR (CsI, cm^{-1}): ν(Cu−S), 381; ν(S−C), 993; ν(C−N), 1499.

dx.doi.org/10.1021/ic300135w | *Inorg. Chem.* 2012, 51, 6577−6591

X-ray Crystallography. Crystals were mounted on glass fibers with epoxy resin, and all geometric and intensity data were collected on a Bruker APEXII CCD diffractometer using graphite monochromated Mo Kα radiation (λ = 0.71073 Å). Data reduction was carried out with SAINT-Plus software.[50] An empirical absorption correction was applied using the SADABS program.[51] Structures were solved by direct methods and refined by full-matrix least-squares on F^2 using the SHELXTL software package,[52] incorporated in *SHELXTL*/PC version 5.10.[53] The data collections for crystals of $\mathbf{1_H}$, $\mathbf{2_H}$, $\mathbf{6_H}$, and **7** were performed at 223(2), 100(2), 253(2), and 253(2) K, respectively. The PF_6 anion of $\mathbf{1_H}$ is disordered over two positions, each in 50% occupancy. All Cu atoms in $\mathbf{2_H}$ are disordered over two positions with 50% occupancy, and the PF_6 anion is disordered over two positions with the major component at 75% occupancy. Several carbon and oxygen atoms of the aza-15-crown-5 moiety in $\mathbf{6_H}$ are found to be disordered at the temperature studied. O11, C17, and O22 are refined isotropically the oxygen and carbon atoms (O1, O2, and C18) of the aza-15-crown-5 in **7** are also disordered and refined isotropically. H-atoms of the alkyl side chain or aza-15-crown-5 ligands are placed at idealized positions except for those of the disordered carbon sites. Pertinent crystallographic data are listed in Supporting Information Table S1. Metric data of $\mathbf{1_H}$, $\mathbf{2_H}$, $\mathbf{6_H}$, and $\mathbf{6_H}$ (neutron data) are in Tables **1** and **7** of Table S4 in the Supporting Information.

Neutron Diffraction Details for $\mathbf{6_H}$. Laue data were obtained using the KOALA[54] Laue neutron diffractometer located on a thermal neutron guide at the OPAL reactor source of the Australian Nuclear Science and Technology Organization. Images from the stationary triclinic crystal were collected at 100 K across two series of eleven frames, interimage 17° rotation of the crystal was perpendicular to the incident beam. A data set was reduced from these images corresponding to approximately 80% of the complete unique set to 0.85 < λ < 1.70 Å. The intensities for each set were indexed and processed via the program LAUE1234,[55] and the two sets were merged R_{int} = 0.085 at the LAUE4 processing step. Structure refinement using the CRYSTALS[56] program suite was undertaken commencing from the positions corresponding to the final X-ray derived structural model. Since only the ratios between unit cell dimensions can be determined from the Laue technique, the dimensions found by X-ray diffraction (100 K) were used in the neutron refinement; the ratios and angles observed were consistent with the X-ray values. An initial refinement of all positions and isotropic displacement parameters for the non-H atoms was followed by deletion from the model of all H atom positions. All hydrogen atoms presented here were clearly observed in a difference map as negative density of a magnitude double that of remaining background, and these H atom sites were reintroduced to the model at their observed positions and included in the refinement with isotropic displacement parameters (and in regions of disorder, with fractional occupancy where consistent with the data). Similarity restraints were employed in order to better model the disordered regions at the periphery of the assembly, and light restraints were applied to H-atom geometry around the aza-crown ether rings. There is no residual difference density consistent with any additional atomic sites whether hydrogen or non-hydrogen in crystals of this material except at the periphery of the molecule where disorder of the crown ether related groups is modeled and in the solvent containing region, minimum and maximum residual densities are −1.36 and +1.96.

Due to the inherent weakness of neutron diffraction data compared to X-ray derived data, the number of data above 3σ did not permit the refinement of an anisotropic model and only the Cu and hydride H atoms were modeled anisotropically. Final refinement cycles of 1017 parameters against 4074 reflections (I > 3σI) with 484 restraints converged at R = 0.131, R_w = 0.127. A chebychev polynomial weighting scheme was used and S = 1.00. The hydride H atom coordinated to four Cu atoms of the cluster is clearly determined. All geometries reported for this structure are calculated using the full variance-covariance matrix of the refinement.

Computational Details. Geometry optimizations were carried out using the Gaussian 09 package,[57] employing the PBE1PBE (PBE0) functional,[58] and using the general triple-ξ polarized basis set, namely the Def2-TZVP set from EMSL Basis Set Exchange Library.[59] All stationary points were fully characterized as true mimina via analytical frequency calculations. The geometries obtained from DFT calculations were used to perform natural orbital population analysis by the NBO 5.0 program.[60] The composition of the molecular orbitals is calculated using the AOMix program.[61] The UV−visible transitions were calculated by means of time-dependent DFT (TDDFT) calculations,[62] using the same PBE0 functional, but with a smaller basis set, namely the general double-ξ polarized LANL2DZ basis set[63a−d] augmented with Ahlrichs polarization functions on all atoms,[63e] in order to reduce the computational demand. It has been checked before on test calculations that this basis set change does not modify significantly the energy of the first low energy transitions. Only singlet−singlet, i.e. spin-allowed, transitions have been computed. The UV−visible spectra were simulated from the computed TDDFT transitions and their oscillator strengths by using the SWizard program,[64] each transition being associated with a Gaussian function of half-height width equal to 3000 cm^{-1}. The gauge including atomic orbital (GIAO)[65] method has been used to compute the 1H chemical shifts, $\delta = \sigma_{TMS} - \sigma_{cluster}$, where σ_{TMS} and $\sigma_{cluster}$ are, respectively, the isotropic chemical shielding of $\mathbf{1_H}$ in tetramethylsilane and of the encapsulated hydride in the $[Cu_8(H)(S_2CNH_2)_6]^+$ cluster.

■ ASSOCIATED CONTENT

Ⓢ Supporting Information

X-ray crystallographic files in CIF format for compounds $\mathbf{1_H}$, $\mathbf{2_H}$, $\mathbf{6_H}$ (X-ray structure), $\mathbf{6_H}$ (neutron structure), and **7** (CCDC-847804−847808); Figure S1−S5; crystallographic data (Table S1, S2, and S4); and Cartesian coordinates of all the DFT computed models (Table S3). This material is available free of charge via the Internet at http://pubs.acs.org.

■ AUTHOR INFORMATION

Corresponding Author

*E-mail: chenwei@mail.ndhu.edu.tw (C.W.L.), jean-yves.saillard@univ.rennes1.fr (J.-Y.S.).

Notes

The authors declare no competing financial interest.

■ ACKNOWLEDGMENTS

Financial supports from the National Science Council of Taiwan (NSC 100-2113-M-259-003) and the Institut Universitaire de France (IUF) are gratefully acknowledged. Travel facilities were provided through the French-Taiwanese ORCHID project no. 19667PA. The award of neutron beam access at ANSTO to Proposal 1177 is likewise acknowledged. We thank professor Yuan-Jann Chen of Fu-Jen Catholic University for the lifetime measurements.

■ REFERENCES

(1) (a) *Transition Metal Hydrides*; Dedieu, A., Ed.; VCH: New York, 1992. (b) Esteruelas, M. A.; Oro, L. A. *Chem. Rev.* **1998**, *98*, 577−588. (c) Hoskin, A. J.; Stephan, D. W. *Coord. Chem. Rev.* **2002**, *233*−*234*, 107−129. (d) McGrady, G. S.; Guilera, G. *Chem. Soc. Rev.* **2003**, *32*, 383−392. (e) Konkol, M.; Okuda, J. *Coord. Chem. Rev.* **2008**, *252*, 1577−1591.

(2) (a) *Recent Advances in Hydride Chemistry*; Peruzzini, M.; Poli, R., Eds.; Elsevier: New York, 2001. (b) Maeland, A. J. In *Recent Advances in Hydride Chemistry*; Peruzzini, M.; Poli, R., Eds.; Elsevier: New York, 2001; pp 531−556.

(3) (a) Adams, R. D.; Captain, B.; Smith, M. D. *Angew. Chem., Int. Ed.* **2006**, *45*, 1109−1112. (b) Brayshaw, S. K.; Ingleson, M. J.; Green, J. C.; Raithby, P. R.; Kociok-Köhn, G.; McIndoe, J. S.; Weller, A. S. *Angew. Chem., Int. Ed.* **2005**, *44*, 6875−6878. (c) Brayshaw, S. K.; Ingleson, M. J.; Green, J. C.; McIndoe, J. S.; Raithby, P. R.; Kociok-Köhn, G.; Weller, A. S. *J. Am. Chem. Soc.* **2006**, *128*, 6247−6263.

(d) Shima, T.; Luo, Y.; Stewart, T.; Bau, R.; McIntyre, G. J.; Mason, S. A.; Hou, Z. *Nature Chem.* **2011**, *3*, 814−820.
(4) Köhn, R. D.; Pan, Z.; Mahon, M. F.; Kociok-Köhn, G. *Chem. Commun.* **2003**, 1272−1273.
(5) Kamiguchi, S.; Imoto, H.; Saito, T.; Chihara, T. *Inorg. Chem.* **1998**, *37*, 6852−6857.
(6) Adams, R. D.; Babin, J. E.; Tanner, J. T. *Organometallics* **1988**, *7*, 2027−2033.
(7) Jackson, P. F.; Johnson, B. F. G.; Lewis, J.; Raithby, P. R.; Mcpartlin, M.; Nelson, W. J. H.; Rouse, K. D.; Alibon, J.; Mason, S. A. *J. Chem. Soc., Chem. Commun.* **1980**, 295−297.
(8) (a) Hart, D. W.; Teller, R. G.; Wei, C.-Y.; Bau, R.; Longoni, G.; Campanella, S.; Chini, P.; Koetzle, T. F. *J. Am. Chem. Soc.* **1981**, *103*, 1458−1466. (b) Hart, D. W.; Teller, R. G.; Wei, C.-Y.; Bau, R.; Longoni, G.; Campanella, S.; Chini, P.; Koetzle, T. F. *Angew. Chem., Int. Ed. Engl.* **1979**, *18*, 80−81.
(9) Broach, B. W.; Dahl, L. F.; Longoni, G.; Chini, P.; Schultz, A. J.; Williams, J. M. In *Transition Metal Hydrides*, Advances in Chemistry Series; Bau, R., Ed.; 1978, Vol. *167*, Chapter 7.
(10) Yousufuddin, M.; Gutmann, M. J.; Baldamus, J.; Tardif, O.; Hou, Z.; Mason, S. A.; Mclntyre, G. J.; Bau, R. *J. Am. Chem. Soc.* **2008**, *130*, 3888−3891.
(11) (a) Luo, Y.; Baldamus, J.; Tardif, O.; Hou, Z. *Organometallics* **2005**, *24*, 4362−4266. (b) Stewart, T.; Nishiura, M.; Konno, Y.; Hou, Z.; Mcintyre, G. J.; Bau, R. *Inorg. Chim. Acta* **2010**, *363*, 562−566.
(12) Cheng, J.; Saliu, K.; Kiel, G. Y.; Ferguson, M. J.; McDonald, R.; Takats, J. *Angew. Chem., Int. Ed.* **2008**, *47*, 4910−4913.
(13) Tanaka, S.; Dubs, C.; Inagaki, A.; Akita, M. *Organometallics* **2005**, *24*, 163−184.
(14) Shima, T.; Hou, Z. *Dalton Trans.* **2010**, *39*, 6858−6963.
(15) Serrano, C. B.; Less, R. J.; Mcpartlin, M.; Naseri, V.; Wright, D. S. *Organometallics* **2010**, *29*, 5754−5756.
(16) (a) Budzichowski, T. A.; Chisholm, M. H.; Huffman, J. C.; Eisenstein, O. *Angew. Chem., Int. Ed. Engl.* **1994**, *33*, 191−193. (b) Budzichowski, T. A.; Chisholm, M. H.; Huffman, J. C.; Kramer, K. S.; Eisenstein, O. *J. Chem. Soc., Dalton Trans.* **1998**, 2563−2568.
(17) Kamiguchi, S.; Saito, T.; Honda, Z. *J. Organomet. Chem.* **2000**, *609*, 184−188.
(18) Eady, C. R.; Jackson, P. F.; Johnson, B. F. G.; Lewis, J.; Carlotta, M.; Mcpartlin, M.; Nelson, W. J. *J. Chem. Soc., Dalton Trans.* **1980**, 383−392.
(19) (a) Eguchi, T.; Heaton, B. T.; Harding, R.; Miyagi, K.; Longoni, G.; Nähring, J.; Nakamura, N.; Nakayama, H.; Pakkanen, T. A.; Pursiainen, J.; Smith, A. K. *J. Chem. Soc., Dalton Trans.* **1996**, 625−630. (b) Eguchi, T.; Heaton, B. T. *J. Chem. Soc., Dalton Trans.* **1999**, 3523−3530.
(20) Li, X.-F.; Baldamus, J.; Nishiura, M.; Tardif, O.; Hou, Z. *Angew. Chem., Int. Ed.* **2006**, *45*, 8184−8188.
(21) (a) Liao, P.-K.; Sarkar, B.; Chang, H.-W.; Wang, J.-C.; Liu, C.-W. *Inorg. Chem.* **2009**, *48*, 4089−4097. (b) Liu, C. W.; Sarkar, B.; Huang, Y.-J.; Liao, P.-K.; Wang, J.-C.; Saillard, J.-Y.; Kahal, S. *J. Am. Chem. Soc.* **2009**, *131*, 11222−11233. (c) Liu, C. W.; Chang, H.-W.; Sarkar, B.; Saillard, J.-Y.; Kahlal, S.; Wu, Y.-Y. *Inorg. Chem.* **2010**, *49*, 468−475. (d) Liu, C. W.; Chang, H.-W.; Fang, C.-S.; Sarkar, B.; Wang, J.-C. *Chem. Commun.* **2010**, *46*, 4571−4573.
(22) Liao, P.-K.; Liu, K.-G.; Fang, C.-S.; Liu, C. W.; Fackler, J. P., Jr.; Wu, Y.-Y. *Inorg. Chem.* **2011**, *50*, 8410−8417.
(23) Casanova, D.; Llunell, M.; Alemany, P.; Alvarez, S. *Chem.—Eur. J.* **2005**, *11*, 1479−1494.
(24) Cardell, D.; Horgarth, G.; Faulkner, S. *Inorg. Chim. Acta* **2006**, *359*, 1321−1324.
(25) Hogarth, G. In *Progress in Inorganic Chemistry*, Karlin, K. D., Ed; John Wiley & Sons, Inc.: New York, 2005; Vol *53*, pp 71−560.
(26) Bondi, A. *J. Phys. Chem.* **1964**, *68*, 441−445.
(27) Cordero, B.; Gomez, V.; Platero-Prates, A. E.; Reves, M.; Echeverria, J.; Cremades, E.; Barragan, F.; Alvarez, S. *Dalton Trans.* **2008**, 2832−2838.
(28) (a) Berg, J. M.; Holm, R. H. In *Metal Ions in Biology*, Spiro, T. G., Ed.; Wiley-Interscience: New York, 1982; Vol *4*, Chapter 1. (b) Holm, R. H.; Ciurli, S.; Weigel, J. A. In *Progress in Inorganic Chemistry: Bioinorganic Chemistry*; Lippard, S. J., Ed.; John Wiley & Sons, Inc.: New York, 1990; Vol *38*, p 1.
(29) Liu, P.; Lightstone, J. M.; Patterson, M. J.; Rodrigues, J. A.; Muckerman, J. T.; White, M. G. *J. Phys. Chem. B* **2006**, *110*, 7449−7455.
(30) (a) Adams, R. D.; Boswell, E. M.; Captain, B. *Organometallics* **2008**, *27*, 1169−1173. (b) Stark, J. L.; Harms, B.; Guzmann-Jimenez, I.; Whitmire, K. H.; Gautier, R.; Halet, J.-F.; Saillard, J.-Y. *J. Am. Chem. Soc.* **1999**, *121*, 4409−4418.
(31) Stephan, H.-O.; Kanatzidis, M. G.; Henkel, G. *Angew. Chem., Int. Ed. Engl.* **1996**, *35*, 2135−2137.
(32) Preut, H.; Haupt, H.-J. *Acta Crystallogr., Sect. B* **1979**, *35*, 1205−1207.
(33) Stevens, R. C.; McLean, M. R.; Bau, R.; Koetzle, T. F. *J. Am. Chem. Soc.* **1989**, *111*, 3472−3473.
(34) (a) Wang, C.; Haushalter, R. C. *Inorg. Chim. Acta* **1999**, *288*, 1−6. (b) Wang, C.; Haushalter, R. C. *Chem. Commun.* **1997**, 1457−1458.
(35) Fenske, D.; Hachgenei, J.; Ohmer, J. *Angew. Chem., Int. Ed. Engl.* **1985**, *24*, 706−709.
(36) Bateman, L. W.; Green, M.; Howard, J. A. K.; Mead, K. A.; Mills, R. M.; Dalter, I. D.; Stone, F. G. A.; Woodward, P. *J. Chem. Soc., Chem. Commun.* **1982**, 773−775.
(37) Bruce, M. I.; Nicholson, B. K. *J. Chem. Soc., Chem. Commun.* **1982**, 1141−1143.
(38) Whitmire, K. H. *J. Am. Chem. Soc.* **1985**, *107*, 1056−1057.
(39) Al-Mandhary, M. R. A.; Buntem, R.; Doherty, C. L.; Edwards, A. J.; Gallagher, J. F.; Lewis, J.; Li, C.-K.; Raithby, P. R.; Ramire de Arellano, M. C.; Shields, G. P. *J. Clust. Sci.* **2005**, *16*, 127−150.
(40) (a) Granell, J.; Green, M. L. H.; Lowe, V. J.; Marder, S. R.; Mountford, P.; Saunders, G. C.; Walker, N. M. *J. Chem. Soc., Dalton Trans.* **1990**, 605−614. (b) Jian, F.-F.; Wang, Z.-X.; Bai, Z.-P.; You, X.-Z.; Fun, H.-K.; Chinnakali, K.; Razak, I. A. *Polyhedron* **1999**, *18*, 3401−3406. (c) Giovagnini, L.; Sitran, S.; Montopoli, M.; Caparrotta, L.; Corsini, M.; Rosani, C.; Zanello, P.; Dou, Q. P.; Fregona, D. *Inorg. Chem.* **2008**, *47*, 6336−6343.
(41) Connelly, N. G.; Geiger, W. E. *Chem. Rev.* **1996**, *96*, 877−910.
(42) Sabin, F.; Ryu, C. K.; Ford, P. C.; Vogler, A. *Inorg. Chem.* **1992**, *31*, 1941−1945.
(43) Plyusnin, V. F.; Kolomeets, A. V.; Grivin, V. P.; Larionov, S. V.; Lemmetyinen, H. *J. Phys. Chem. A* **2011**, *115*, 1763−1773 and references therein.
(44) Garland, M. T.; Halet, J.-F.; Saillard, J.-Y. *Inorg. Chem.* **2001**, *40*, 3342−3350.
(45) (a) Miertuš, S.; Scrocco, E.; Tomasi, J. *Chem. Phys.* **1981**, *55*, 117−129. (b) Cossi, M.; Rega, N.; Scalmani, G.; Barone, V. J. *Comput. Chem.* **2003**, *24*, 669−681.
(46) Liu, C. W. unpublished results.
(47) Kubas, G. J. *Inorg. Synth.* **1979**, *19*, 90−112.
(48) (a) Kaugars, G.; Rizzo, V. L. *J. Heterocycl. Chem.* **1981**, *18*, 411−412. (b) Green, M. L. H.; Marder, S. R.; Saunders, G. C.; Walker, N. M. *J. Chem. Soc., Dalton Trans.* **1988**, 1697−1700.
(49) Chen, Y.-J.; Xie, P.; Endicott, J. F. *J. Phys. Chem.* **2004**, *108*, 5041−5049.
(50) *SAINT V4.043: Software for the CCDC Detector System*; Bruker Analystic X-ray System: Madison, WI, 1995.
(51) Sheldrick, G. M. *SADABS*; University of Gottingen: Gottingen, Germany, 1996.
(52) Sheldrick, G. M. *Acta Crystallogr.* **2008**, *A64*, 112−122.
(53) *SHELXL 5.10 (PC version): Program Library for Structure Solution and molecular Graphics*; Bruker Analytical X-ray System: Madison, WI, 1998.
(54) Edwards, A. J. *Aust. J. Chem.* **2011**, *64*, 869−872.
(55) Piltz, R. O. *Acta Crystallogr.* **2011**, *A67*, C155.
(56) Betteridge, P. W.; Carruthers, J. R.; Cooper, R. I.; Prout, K.; Watkin, D. J. *J. Appl. Crystallogr.* **2003**, *36*, 1487.
(57) Frisch, M. J.; Trucks, G. W.; Schlegel, H. B.; Scuseria, G. E.; Robb, M. A.; Cheeseman, J. R.; Montgomery, J. A. Jr.; Vreven, T.; Kudin, K. N.; Burant, J. C.; Millam, J. M.; Iyengar, S. S.; Tomasi, J.;

Barone, V.; Mennucci, B.; Cossi, M.; Scalmani, G.; Rega, N.; Petersson, G. A.; Nakatsuji, H.; Hada, M.; Ehara, M.; Toyota, K.; Fukuda, R.; Hasegawa, J.; Ishida, M.; Nakajima, T.; Honda, Y.; Kitao, O.; Nakai, H.; Klene, M.; Li, X.; Knox, J. E.; Hratchian, H. P.; Cross, J. B.; Adamo, C.; Jaramillo, J.; Gomperts, R.; Stratmann, R. E.; Yazyev, O.; Austin, A. J.; Cammi, R.; Pomelli, C.; Ochterski, J. W.; Ayala, P. Y.; Morokuma, K.; Voth, G. A.; Salvador, P.; Dannenberg, J. J.; Zakrzewski, V. G.; Dapprich, S.; Daniels, A. D.; Strain, M. C.; Farkas, O.; Malick, D. K.; Rabuck, A. D.; Raghavachari, K.; Foresman, J. B.; Ortiz, J. V.; Cui, Q.; Baboul, A. G.; Clifford, S.; Cioslowski, J.; Stefanov, B. B.; Liu, G.; Liashenko, A.; Piskorz, P.; Komaromi, I.; Martin, R. L.; Fox, D. J.; Keith, T.; Al-Laham, M. A.; Peng, C. Y.; Nanayakkara, A.; Challacombe, M.; Gill, P. M. W.; Johnson, B.; Chen, W.; Wong, M. W.; Gonzalez, C.; Pople, J. A. *Gaussian 03*, revision B. 04; Gaussian, Inc.: Pittsburgh, PA, 2003.

(58) (a) Perdew, J. P.; Ernzerhof, M.; Burke, K. *J. Chem. Phys.* **1996**, *105*, 9982−9985. (b) Perdew, J. P.; Burke, K.; Ernzerhof, M. *Phys. Rev. Lett.* **1996**, *77*, 3865−3868. (c) Perdew, J. P.; Burke, K.; Ernzerhof, M. *Phys. Rev. Lett.* **1997**, *78*, 1396.

(59) Weigend, F.; Ahlrichs, R. *Phys. Chem. Chem. Phys.* **2005**, *7*, 3297−3305.

(60) Glendening, E. D.; Badenhoop, J. K.; Reed, A. E.; Carpenter, J. E.; Bohmann, J. A.; Morales, C. M.; Weinhold, F. Theoretical Chemistry Institute, University of Wisconsin, Madison, WI, 2001, http://www.chem.wisc.edu/~nbo5.

(61) Gorelsky, S. I. AOMix program, http://www.sg-chem.net/

(62) Burke, K.; Gross, E. K. U. In *A guided tour of Time-Dependent Density Functional Theory, in Density Functionals: Theory and Applications*; Joubert, D., Ed.; Springer: New York, 1998; Vol *500*.

(63) (a) Dunning Jr., T. H.; Hay, P. J. In *Methods of Electronic Structure Theory*; Schaeffer, H. F., Ed.; Plenum Press: New York, 1977. (b) Hay, P. J.; Wadt, W. R. *J. Chem. Phys.* **1985**, *82*, 270−283. (c) Hay, P. J.; Wadt, W. R. *J. Chem. Phys.* **1985**, *82*, 284−298. (d) Hay, P. J.; Wadt, W. R. *J. Chem. Phys.* **1985**, *82*, 299−310. (e) Schafer, A.; Horn, H.; Ahlrichs, R. *J. Chem. Phys.* **1992**, *97*, 2571−2577.

(64) Gorelsky, S. I. *SWizard program*, revision 4.5, http://www.sg-chem.net/.

(65) (a) London, F. *J. Phys. Radium* **1937**, *8*, 397−409. (b) McWeeny, R. *Phys. Rev.* **1962**, *126*, 1028−1034. (c) Ditchfield, R. *Mol. Phys.* **1974**, *27*, 789−807. (d) Dodds, J. L.; McWeeny, R.; Sadlej, A. J. *Mol. Phys.* **1977**, *34*, 1779−1791. (e) Wolinski, K.; Hinton, J. F.; Pulay, P. *J. Am. Chem. Soc.* **1990**, *112*, 8251−8260.